

Angular correlations near the Fermi energy

D. Fox, D. A. Cebra, J. Karn, C. Parks, A. Pradhan, A. Vander Molen,
J. van der Plicht, G. D. Westfall, and W. K. Wilson

National Superconducting Cyclotron Laboratory, Michigan State University, East Lansing, Michigan 48824

R. S. Tickle

Department of Physics, University of Michigan, Ann Arbor, Michigan 48109

(Received 2 July 1987)

Angular correlations between light particles have been studied to probe the extent to which a thermally equilibrated system is formed in heavy ion collisions near the Fermi energy. Single-light-particle inclusive energy spectra and two-particle large-angle correlations were measured for 40 and 50 MeV/nucleon C + C, Ag, and Au. The single-particle inclusive energy spectra are well fit by a three moving source parametrization. Two-particle large-angle correlations are shown to be consistent with emission from a thermally equilibrated source when the effects of momentum conservation are considered. Single-particle inclusive spectra and light-particle correlations at small relative momentum were measured for 35 MeV/nucleon N + Ag. Source radii were extracted from the two-particle correlation functions and were found to be consistent with previous measurements using two-particle correlations and the coalescence model. The temperature of the emitting source was extracted from the relative populations of states using the quantum statistical model and was found to be $4.8_{-2.4}^{+2.8}$ MeV, compared to the 14 MeV temperature extracted from the slopes of the kinetic energy spectra.

I. INTRODUCTION

The extent to which thermalization occurs in intermediate and relativistic energy heavy ion nuclear physics has been the focus of many experiments in the last decade. At relativistic energies single-particle inclusive spectra of light particles were found to be thermal in appearance, leading to the introduction of the fireball model.^{1,2} The basic idea behind the fireball model is that the region of overlap between the projectile and target forms a hot source moving at a velocity slightly less than half the beam velocity. The source expands and emits particles with Maxwell-Boltzmann type energy distributions. In addition, the spectra of light nuclei ($d, t, {}^3\text{He}, {}^4\text{He}$) were found to be well described by the coalescence model.^{2,3} In the coalescence model composite fragments are formed when nucleons are emitted close together in phase space.

At intermediate energies, $20 < E_{\text{beam}} < 200$ MeV/nucleon, single-particle inclusive spectra were measured for light and intermediate mass particles and found again to be well described by a Maxwell-Boltzmann-type energy distribution indicating the formation of a thermal source.⁴⁻⁶ Additional evidence for a thermal source was found in the behavior of the d/p and ${}^4\text{He}/p$ ratios,⁴ which were found to be in general agreement with calculations using the fireball model.^{1,2} Intermediate mass particles have been shown to come from the same source as the light nuclei.⁵ In addition, the coalescence model, which had previously been applied at relativistic energies^{2,3} and at lower energies⁷ to light nuclei, was extended to both light and intermediate mass fragments⁸ at intermediate energies. The extracted coalescence and source

radii showed little variation with fragment mass indicating a common origin for the observed particles. Particles detected in coincidence with intermediate rapidity fragments and projectile-like fragments were also found to come from the same source.⁹ Particles in coincidence with projectile-like fragments very close to the beam mass were found, however, to have a slower source velocity by about 30%, but the source temperature was found to be the same as the temperature extracted from the singles spectra.

While single-particle inclusive kinetic energy spectra of light and intermediate mass fragments have suggested emission of all particles from the same thermally equilibrated intermediate velocity source, some evidence of nonthermal processes has been observed. At relativistic energies quasi-elastic p - p scattering has been seen.¹⁰⁻¹² Other two-particle correlations have suggested that momentum conservation plays a key role in intermediate energy reactions.¹³⁻¹⁷ More recently experiments have sought to measure the temperature of the intermediate source by measuring the relative populations of various nuclear states.¹⁸⁻²⁵ For a system in chemical equilibrium, the ratio of the populations of two states is given by

$$R = \frac{2j_2 + 1}{2j_1 + 1} e^{-(E_2^* - E_1^*)/T}, \quad (1)$$

where j_1 and j_2 are the spins of the two states, E_1^* and E_2^* are the excitation energies of the states, and T is the temperature.

The temperatures extracted from the populations of nuclear states have been shown to be considerably lower than the temperatures extracted from the kinetic energy spectra. Morrissey *et al.* showed that for 35

MeV/nucleon N + Ag the populations of γ -ray emitting states indicated a temperature less than 1 MeV, while the temperature extracted from the kinetic energy spectra was 10 MeV.^{18,19} More recently, the method of Morrissey *et al.* has been extended to particle unstable states of light nuclei.^{22–24} For the system 35 MeV/nucleon N + Au,²² temperatures of between 3 and 9 MeV were extracted from the particle unstable states of ${}^6\text{Li}$. The higher temperatures were obtained for higher total energy of the emitted ${}^6\text{Li}$ parent nuclei. Temperatures were also extracted for particle unstable states in ${}^5\text{Li}$ and ${}^6\text{Li}$ in coincidence with fission fragments.²³ The extracted temperatures were shown to be about 5 MeV independent of the folding angle of the two fission fragments. The populations of particle unstable states have also been measured for 60 MeV/nucleon Ar + Au.²⁴ Temperatures of 4.6 ± 0.7 and 4.2 ± 0.5 MeV were extracted from widely separated states in ${}^5\text{Li}$ and ${}^8\text{Be}$. In addition, a temperature of about 5.5 MeV was obtained using a global fit to the populations of all the measured stable and unstable states using the quantum statistical model.

In order to probe the extent to which a thermally equilibrated source is created in heavy-ion reactions around the Fermi energy we have performed two experiments. In the first experiment single-particle inclusive kinetic energy spectra and two-particle large-angle correlations of light nuclei were studied for 40 and 50 MeV/nucleon C-induced reactions on C, Ag, and Au targets. The measured single-particle inclusive energy spectra are fit using a three moving source fit. A momentum conservation model is used to determine the extent to which energy and momentum conservation effects the measured two-particle correlations.

In the second experiment the populations of particle unstable states were measured for 35 MeV/nucleon N-induced reactions on an Ag target using two-particle correlations at small relative momentum. The populations of particle unstable states are extracted from the two-particle correlations. The quantum statistical model is used to extract the source temperature for 35 MeV/nucleon N + Ag from the populations of the particle bound and unbound states measured in the present work combined with the data of Morrissey and Bloch for the γ - and neutron-emitting states. In addition, information about the space-time extent of the emitting system is extracted from the two-particle correlation functions.

II. EXPERIMENTAL SETUP

Both experiments were performed using beams from the K500 Superconducting Cyclotron at Michigan State University. Large angle correlations were measured for C-induced reactions at 40 and 50 MeV/nucleon. The beam was incident on targets of 26 mg/cm² graphite, 4.0 mg/cm² Ag, and 5.5 mg/cm² Au. The 40 MeV/nucleon beam was used on all three targets while the 50 MeV/nucleon beam was used only on the graphite target. The average beam intensity on the graphite target was 0.5 particle namps, on the other targets the average intensity was 3 particle namps. The experimental setup for the large angle correlation experiment is shown in Fig. 1 and the positions and solid angles of the detectors are given in

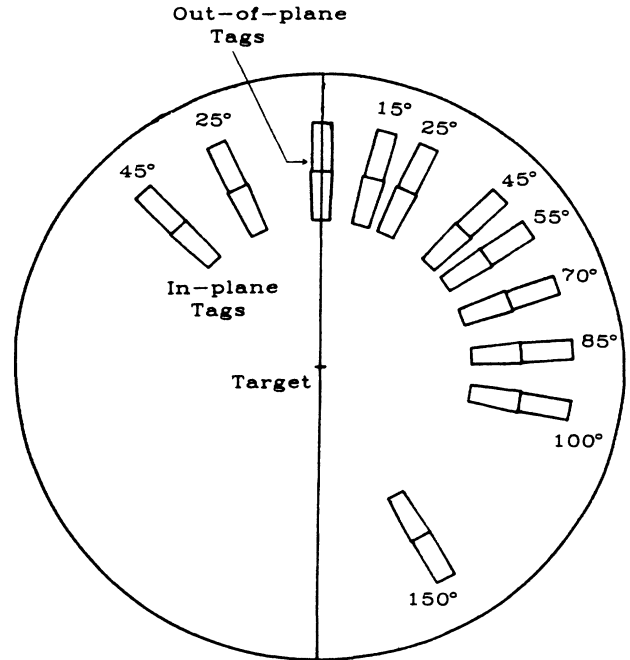


FIG. 1. Chamber setup for large-angle correlation experiment.

Table I. Particle identification and energy measurement were achieved using twelve fast-slow phoswich telescopes. Each telescope consisted of a 1.6 mm thick fast plastic (BC-412) ΔE detector optically coupled to a 127 mm long slow plastic (BC-444) E detector. Two pairs of telescopes were used as tag counters and eight telescopes were used as array counters. One pair of tag telescopes was placed at $\theta = 45^\circ$ with $\Phi = 180^\circ$ and 90° . The second pair of tag telescopes was placed at $\theta = 25^\circ$ with the same azimuthal angles as the first pair. The tag telescopes at $\Phi = 180^\circ$ were designated as the in-plane tag telescopes and the pair at $\Phi = 90^\circ$ were called the out-of-plane tag telescopes. The nine array telescopes were placed at angles ranging from $\theta = 15^\circ$ to $\theta = 150^\circ$ with $\Phi = 0^\circ$.

TABLE I. Telescope positions and solid angles for the large-angle correlation measurement.

Telescope	θ (deg)	Φ (deg)	Solid angle (msr)
In-plane tag 1	25	180	1.22
In-plane tag 2	45	180	2.41
Out-of-plane tag 1	25	90	1.22
Out-of-plane tag 2	45	90	2.41
Array telescope 1	15	0	1.02
Array telescope 2	25	0	1.22
Array telescope 3	45	0	2.41
Array telescope 4	55	0	1.02
Array telescope 5	70	0	2.41
Array telescope 6	85	0	2.41
Array telescope 7	100	0	2.41
Array telescope 8	150	0	2.41

The unstable resonance experiment was performed using a beam of 35 MeV/nucleon ^{14}N incident on a target of 1.6 mg/cm^2 Ag. Two types of detectors were used in the unstable resonance experiment. Particle identification and energy measurement were achieved using sixteen fast-slow phoswich telescopes stacked in a 4×4 array. The sixteen telescopes used in this experiment were of the type used in the large angle correlation experiment. Each phoswich had an opening angle of 5.7° and the entire array had a solid angle of 165 msr. To improve further the angular resolution of the array, a multiwire proportional counter (MWPC) was placed in front of the phoswich array. The MWPC contained three wire planes, two at right angles with respect to each other and the third at 45° with respect to the first two planes in order to resolve possible ambiguities in events with more than one particle. The wire spacing of this counter is 2.5 mm, but the wires are paired together giving an effective spacing of 5 mm to provide an angular resolution of 0.7° . Data were taken with the MWPC at central angles of $\theta = 35^\circ, 45^\circ, 60^\circ,$ and 80° .

The kinetic energy spectra of the bound states of the He, Li, and Be isotopes studied in the unstable resonance experiment were measured in a separate experiment using a single two element Si stack. The stack consisted of a $400\text{-}\mu\text{m}$ ΔE detector and a 5-mm E detector and had a

TABLE II. Telescope energy ranges for unstable resonance singles measurement.

Particle	Low energy cut (MeV)	High energy cut (MeV)
^3He	26	111
^4He	29	126
^6He	35	151
^6Li	54	237
^7Li	59	254
^7Be	80	350
^9Be	92	392
^{10}Be	95	411

solid angle of 1.54 msr. Data were taken at the same angles, $\theta = 35^\circ, 45^\circ, 60^\circ,$ and 80° , measured in the unstable resonance measurement. The energy range measured for each isotope is given in Table II.

The phoswich telescopes used in both experiments were calibrated using beams of deuterons and alphas following each experiment. The silicon detectors used in the singles measurement for the unstable resonance experiment were calibrated using calibrated pulsers.

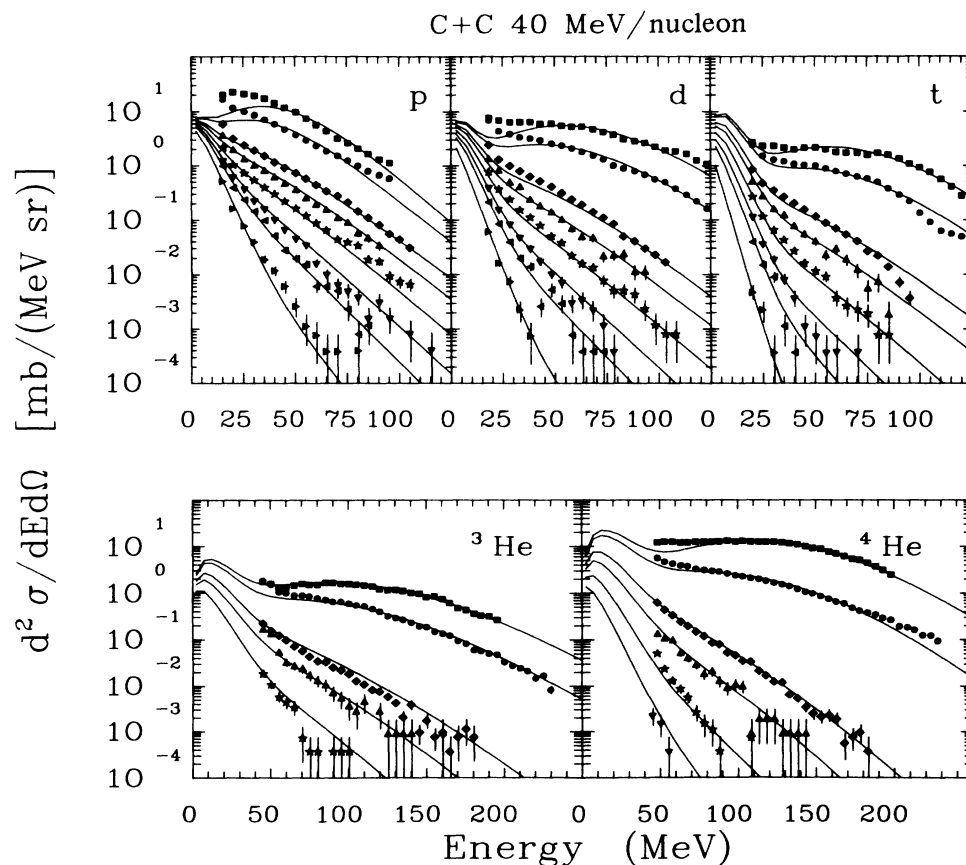


FIG. 2. Light-particle energy spectra for 40 MeV/nucleon C + C. The angles are $15^\circ, 25^\circ, 45^\circ, 55^\circ, 70^\circ, 85^\circ, 100^\circ,$ and 150° . The lines are the results of moving source fits.

III. LARGE-ANGLE CORRELATIONS

A. Light-particle inclusive kinetic energy spectra

Representative inclusive energy spectra for p , d , t , ${}^3\text{He}$, and ${}^4\text{He}$ for 40 MeV/nucleon C + C and Au are shown in Figs. 2 and 3, for $\theta = 15^\circ, 25^\circ, 45^\circ, 55^\circ, 70^\circ, 85^\circ, 100^\circ,$ and 150° . The spectra for the other systems have been presented previously.²⁶ The spectra have been corrected for reaction losses in the phoswiches, and the errors shown are statistical. The spectra are smooth, decreasing monotonically with increasing angle and decaying exponentially at high energies, suggesting a thermal origin for the observed particles. The spectra show signs of emission from a fast projectile-like source at the forward angles, $\theta = 15^\circ$ and 25° . At low energies there is evidence of emission from a slow target-like source.

B. Moving source parametrization

We have fitted the data with a triple moving source parametrization, which assumes the presence of a projectile-like source, a target-like source, and an intermediate velocity source. All three sources are assumed to move in the beam direction. While it is true that at 40–50 MeV/nucleon the three sources are not well

separated, the energy spectra show definite signs of each of the three sources. The energy spectra for each source are assumed to be described by a relativistic Maxwell-Boltzmann energy distribution. In the rest frame of each source the distribution is given by

$$\frac{d^2\sigma}{p'^2 dp' d\Omega'} = \frac{\sigma_0}{4\pi m^3} \frac{e^{-E'/\tau}}{2(\tau/m)^2 K_1(m/\tau) + (\tau/m) K_0(m/\tau)}, \quad (2)$$

where p' and E' are the momentum and total energy of a particle in the source rest frame, and K_0 and K_1 are modified Bessel functions of the second kind, and σ_0 and τ are the production cross section and source temperature for the given source. The energy spectra in the lab are then given by

$$\frac{d^2\sigma}{dE d\Omega} = \frac{pE' d^2\sigma}{p'^2 dp' d\Omega'}, \quad (3)$$

where

$$E' = \gamma(E - \beta p \cos\theta_{\text{lab}}), \quad (4)$$

p and E are the momentum and total energy of a particle in the lab frame, θ_{lab} is the lab angle, and β is the velocity

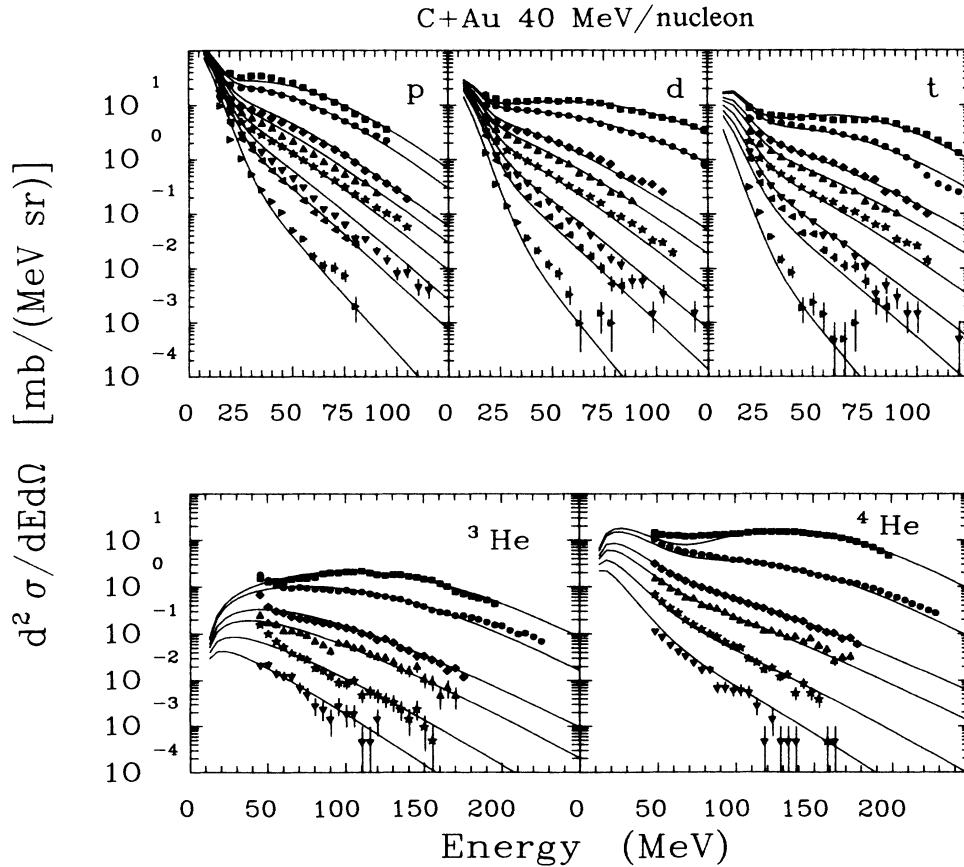


FIG. 3. Light-particle energy spectra for 40 MeV/nucleon C + Au. The angles are $15^\circ, 25^\circ, 45^\circ, 55^\circ, 70^\circ, 85^\circ, 100^\circ,$ and 150° . The lines are the results of moving source fits.

TABLE III. Energy and angle ranges used for moving source fits and the Coulomb shifts for Ag and Au data.

Particle	Target		Target-like		Source Intermediate		Projectile-like	
	Ag V_c (MeV)	Au V_c (MeV)	θ	E (MeV)	θ	E (MeV)	θ	E (MeV)
p	4	5	100–150°	10–50	55–85°	40–125	15–25°	40–125
d	4	5	100–150°	10–50	55–85°	50–125	15–25°	40–150
t	4	5	85–150°	10–50	55–85°	50–75	15–25°	50–100
^3He	5	10	45–70°	40–80	45–70°	80–200	15–25°	80–250
^4He	5	10	45–85°	40–60	45–55°	100–200	15–25°	80–250

of the source in the lab. For each source β , σ_0 , and τ are fit using those angles and energies that are dominated by the source being fit. The angles and energy ranges fit for each source are listed in Table III. Also listed in Table III are the Coulomb shifts that were applied to the Ag and Au data prior to fitting. The fits are shown in Figs. 2 and 3 as lines and the extracted parameters are listed in Table IV. Typical uncertainties are 5–20% for σ_0 , ± 0.002 – 0.007 for β and ± 0.2 – 0.5 MeV for τ . The target-like source was not fitted for the ^3He spectra for the Ag and Au targets. Due to the lack of helium spectra backward of $\theta=85^\circ$, the target-like source for the helium isotopes had to be fit using the low-energy part of the spectra at more forward angles. In addition, the fit for the intermediate source included the 45° spectra for the helium isotopes. The extracted parameters for the heli-

um isotopes have higher velocities and temperatures for the target-like and intermediate sources than do the hydrogen isotopes. For the projectile-like source the helium isotopes have the same velocities as the hydrogen isotopes, but higher temperatures. These differences between the extracted parameters might be due to the different angular and energy ranges used in the fits.

The fits are excellent except for some differences at forward angles for the carbon target. These differences may be caused by the small size of the sources for the C + C system. The intermediate source size with the largest weight ($2\pi b \cdot db \cdot A$) is twelve nucleons.

C. Two-particle in-plane correlations, 45° tag

The two-particle correlations are shown in Figs. 4–8 for p - p , p - d , d - d , d - ^4He , and ^4He - ^4He . The correlations

TABLE IV. Moving source parameters.

Particle	Target-like source			Intermediate source			Projectile-like source		
	Cross section σ_0 (mb)	Velocity β (c)	Temp. τ (MeV)	Cross section σ_0 (mb)	Velocity β (c)	Temp. τ (MeV)	Cross section σ_0 (mb)	Velocity β (c)	Temp. τ (MeV)
40 MeV/nucleon C + C									
p	620	0.016	4.6	472	0.146	11.4	311	0.259	4.9
d	470	0.027	4.3	138	0.124	11.1	215	0.234	5.5
t	460	0.037	3.8	56	0.124	10.3	74	0.201	5.7
^3He	280	0.064	5.5	62	0.152	11.8	95	0.251	9.6
^4He	970	0.071	5.3	260	0.149	9.7	757	0.240	7.0
50 MeV/nucleon C + C									
p	600	0.022	5.3	460	0.174	14.0	361	0.288	5.2
d	380	0.026	4.8	158	0.145	13.0	239	0.267	6.6
t	205	0.047	5.5	99	0.153	8.8	51	0.237	5.5
^3He	350	0.053	6.2	60	0.184	12.7	90	0.291	9.9
^4He	470	0.080	6.8	111	0.165	11.7	652	0.271	7.9
40 MeV/nucleon C + Ag									
p	8200	0.015	3.5	1910	0.129	11.9	760	0.257	6.1
d	1800	0.019	4.2	920	0.123	11.9	411	0.251	7.8
t	800	0.020	4.2	420	0.113	11.7	157	0.210	6.2
^3He				241	0.179	15.4	66	0.278	11.4
^4He	1640	0.063	7.0	808	0.163	16.0	737	0.255	7.0
40 MeV/nucleon C + Au									
p	8700	0.012	3.6	2450	0.123	12.2	670	0.263	6.7
d	2000	0.015	3.8	1020	0.118	12.2	414	0.256	7.5
t	1100	0.031	4.3	480	0.115	13.3	154	0.208	5.3
^3He				162	0.168	17.1	88	0.267	8.7
^4He	1250	0.069	7.7	569	0.154	18.4	866	0.253	6.6

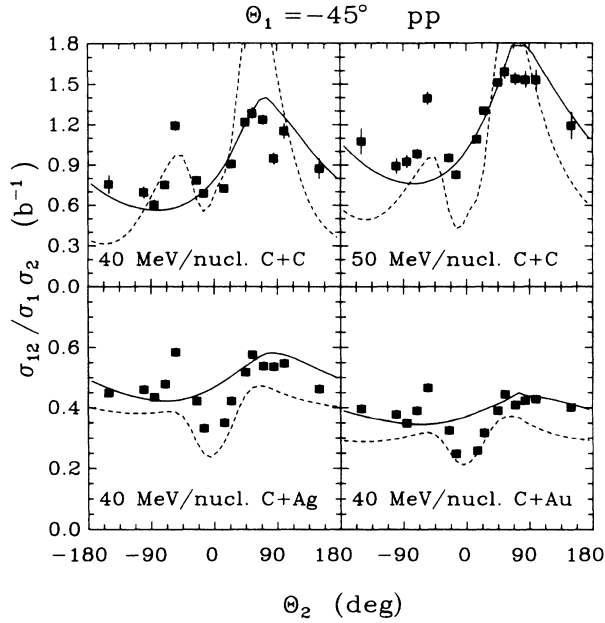


FIG. 4. Two-proton correlation function for which one proton is detected at $\theta_1 = -45^\circ$. The lines are the results of momentum conservation model calculations that are described in the text.

are shown in terms of the two-particle correlation cross section, σ_{12} , divided by the singles cross sections, σ_1 and σ_2 . In each case one of the particles is detected at $\theta_1 = -45^\circ$ and the second particle is detected between $\theta_2 = -150^\circ$ and $+150^\circ$. A negative angle for the second particle means the two particles were observed on the

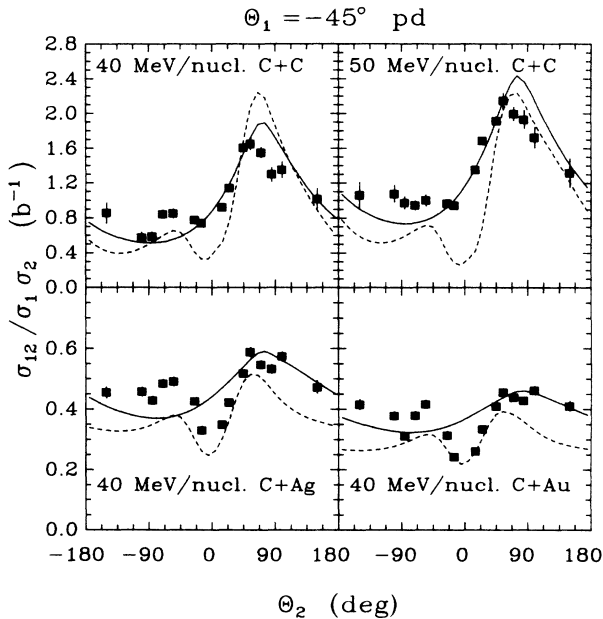


FIG. 5. Proton-deuteron correlation function for which the deuteron is detected at $\theta_1 = -45^\circ$. The lines are the results of momentum conservation model calculations that are described in the text.

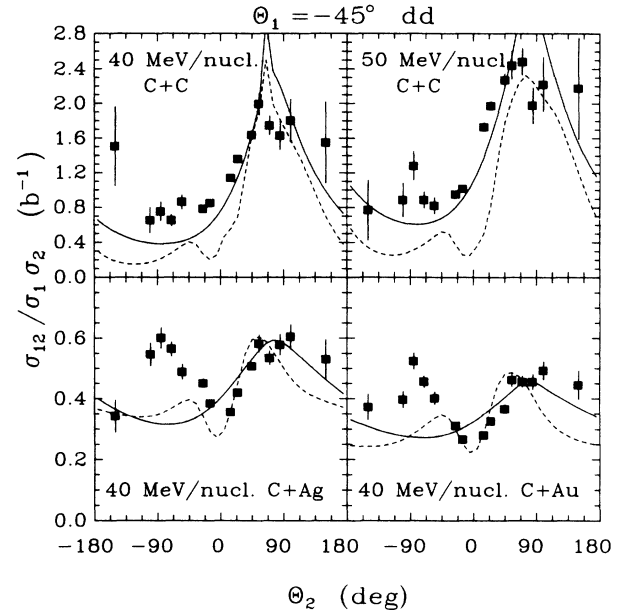


FIG. 6. Two-deuteron correlation function for which one deuteron is detected at $\theta_1 = -45^\circ$. The lines are the results of momentum conservation model calculations that are described in the text.

same side of the beam, while a positive angle indicates emission on opposite sides of the beam. For the nonidentical particle cases (p - d , d - ^4He), the case for which the heavier particle was detected at $\theta_1 = -45^\circ$ is shown. The correlations have been integrated over the energy ranges given in Table V.

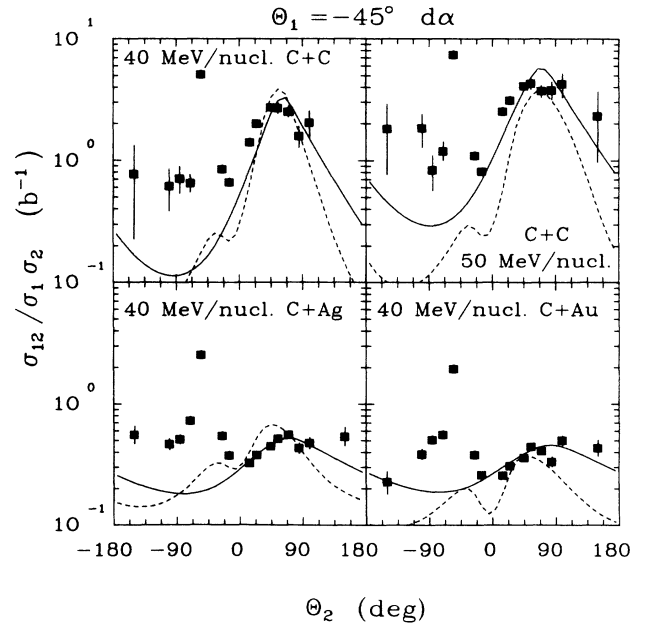


FIG. 7. Deuteron-alpha correlation function for which the alpha is detected at $\theta_1 = -45^\circ$. The lines are the results of momentum conservation model calculations that are described in the text.

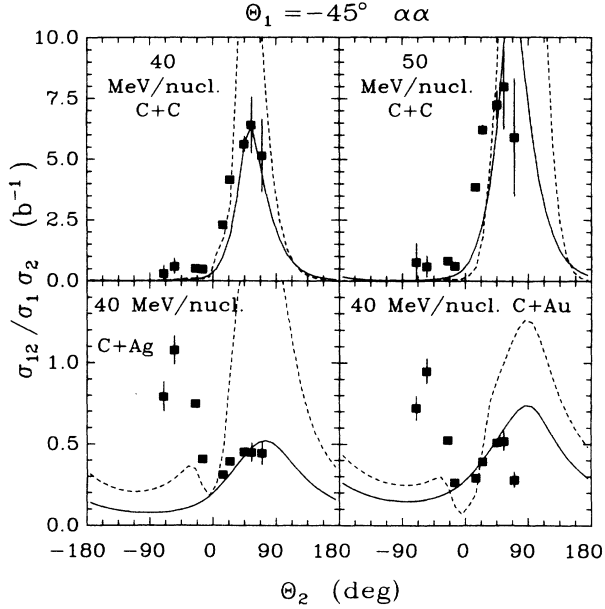


FIG. 8. Two-alpha correlation function for which one alpha is detected at $\theta_1 = -45^\circ$. The lines are the results of momentum conservation model calculations that are described in the text.

In general, the correlations for the C + C systems show a broad maximum at positive angles which indicates a preference for emission of particles to opposite sides of the beam. The magnitude of the peak increases as the mass of the observed particles increases and is slightly larger at 50 MeV/nucleon than at 40 MeV/nucleon. For negative angles the correlations are almost flat as a function of the angle of the second particle. The p - p and d - ${}^4\text{He}$ correlations are exceptions to this trend because they show peaks at $\theta_2 = -55^\circ$. These peaks come from the decay of particle unstable states in ${}^2\text{He}$ and ${}^6\text{Li}$. The C + Ag and C + Au systems have different systematic behavior. The correlation function is in general almost symmetric about $\theta_2 = 0^\circ$ with the same side being only slightly preferred. The p - p peak coming from ${}^2\text{He}$ break up in the light C + C systems is considerably weaker in the heavier systems. Both the d - ${}^4\text{He}$ and ${}^4\text{He}$ - ${}^4\text{He}$ correlations show strong peaks coming from the decay of particle unstable states of ${}^6\text{Li}$ and ${}^8\text{Be}$. The ${}^4\text{He}$ - ${}^4\text{He}$ peak was not observed in the lighter systems because it is difficult to form a ${}^8\text{Be}$ given that the average intermediate velocity source contains only twelve nucleons. The particle pairs that are not shown all exhibit the same characteristics that are seen in Figs. 4–8. The p - t , p - ${}^4\text{He}$, and t - ${}^4\text{He}$ correlations all have peaks at $\theta_2 = -55^\circ$ which comes from the decay of particle unstable states.

D. Momentum conservation model

Energy and momentum conservation effects have been used to explain the observed correlations for small systems at lower energies.^{13,14,17} In order to explore the extent to which our data is affected by conservation laws we have carried out calculations incorporating these effects.

TABLE V. Energy ranges for correlations.

Particle	Energy (MeV)
p	12–80
d	16–80
${}^4\text{He}$	47–135

The calculation^{9,13} assumes emission of two particles from a source of size A nucleons. After the first particle is emitted the source recoils, re-equilibrates, and then emits the second particle. The calculation is repeated with the second particle being emitted first. The two cases are then averaged to produce the final coincidence cross section. The entire calculation is integrated over impact parameter with each impact parameter having a weight $dW = 2\pi b \cdot db \cdot A$ where b is the impact parameter and A is the source size which comes from a fireball model^{1,2} calculation. The calculation is normalized by the total reaction cross section. The parameters listed in Table IV for the intermediate source were used to describe the emitting source.

The results of the momentum conservation calculations are shown in Figs. 4–8 as solid lines. The calculations have been renormalized to the data at $\theta_2 = +45^\circ$ and $+55^\circ$. The calculations do a good job of reproducing the general trends in the data but miss some of the details. In the lighter systems the same side correlations are basically flat, except for those cases that have contributions from the decay of resonances, while the calculation predicts a broad minimum at about $\theta_2 = -80^\circ$. The heavier systems have a “V” shaped dip around $\theta_2 = 0^\circ$, but the calculations show no such dip.

Until now we have assumed that the observed two particle correlations are coming only from the intermediate source although from the inclusive spectra shown in Figs. 2 and 3 it is evident that a substantial fraction of the observed particles comes from sources other than the intermediate source. In Fig. 9(a) the contribution to the deuteron singles cross section from each of the three observed sources is shown for the C + Au system. For small angles the projectile source contributes heavily to the singles cross section while for large angles the target-like source dominates the cross section. Even for small angles for which one would expect the projectile-like source to dominate, the target-like source contributes about ten percent of the total cross section. Figure 9(b) shows the contribution to the two-deuteron coincidence cross section from each of the three sources according to momentum conservation calculations using the parameters for each of the sources given in Table IV. From Fig. 9(b) we can see that adding the contributions of the three sources together will increase the coincidence cross section around $\theta_2 = 0^\circ$ by less than 10% while in Fig. 9(a) we see that the addition of the projectile and target-like sources more than doubles the singles cross sections near $\theta_2 = 0^\circ$. This summation will lead to the dip around 0° which is observed in the data.

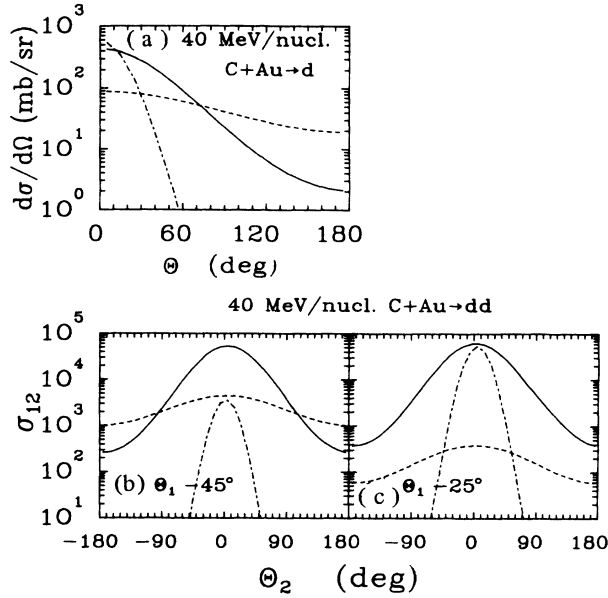


FIG. 9. (a) Contribution from the three sources to the deuteron singles cross section, (b) to the two-deuteron coincidence cross section for $\theta_1 = -45^\circ$, and (c) for $\theta_1 = -25^\circ$ for 40 MeV/nucleon C + Au.

For the lighter systems the effect of the other two sources is somewhat different than for the heavier systems. Figure 10(a) shows the contribution to the deuteron singles cross section for each of the three sources for 40 MeV/nucleon C + C. At forward angles the projectile-like source is far more dominant than it is for C + Au. The projectile-like source is also the leading contributor to the two-deuteron coincidence cross section at the most forward angles as seen in Fig. 10(b) for correlations with $\theta_1 = -45^\circ$. The target-like source contribution to the two-deuteron cross section is peaked at about $\theta_2 = +50^\circ$.

The dashed lines in Figs. 4–8 are the results of three-source momentum conservation calculations. These calculations take into account only correlations between two particles coming from the same source. Unlike the single-source calculation discussed earlier, no normalization has been applied to the three source calculation. The calculation now produces a “V” shape for small θ_2 for the heavier systems. Also, where the single source calculation had a broad minimum for same side correlations, the three source calculation shows a maximum at about $\theta_2 = -55^\circ$. This maximum is almost as large as the opposite side maximum for the heavier systems. The most notable disagreement between the data and the three-source calculation is the underprediction of the coincident cross section for large θ_2 . This disagreement is probably due to correlations between in which one particle comes from the intermediate velocity source and the other particle comes from the target-like source. Correlations involving particles from different sources are not included in the three-source momentum conservation calculation.

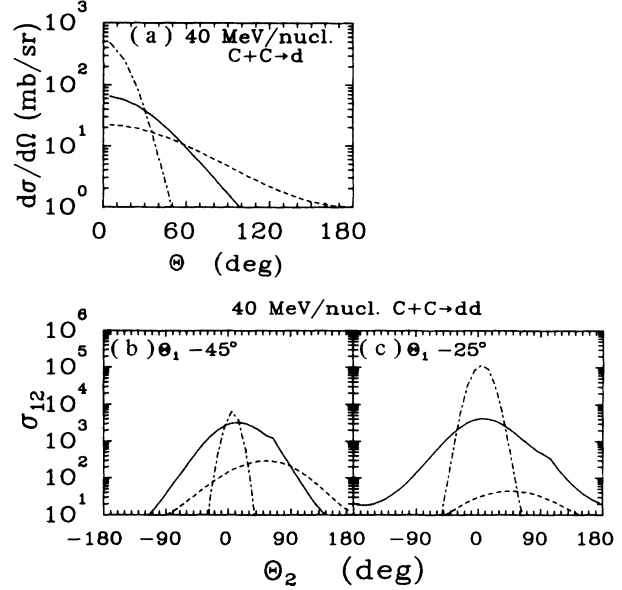


FIG. 10. (a) Contribution from the three sources to the deuteron singles cross section, (b) to the two-deuteron coincidence cross section for $\theta_1 = -45^\circ$, and (c) for $\theta_1 = -25^\circ$ for 40 MeV/nucleon C + C.

E. Two-particle in-plane correlations, 25° tag

The two-particle correlations triggered on a light particle at $\theta_1 = 25^\circ$ are shown in Figs. 11 and 12 for p - p and d - d . The correlations have the same general features as the correlations triggered on the 45° tag telescopes. The light C + C systems show a strong enhancement of the opposite side, while the heavier C + Ag and C + Au systems are symmetric about $\theta_2 = 0^\circ$. There is some evidence in all four systems of an enhancement at $\theta_2 = -15^\circ$ in the p - p correlations.

The lines in Figs. 11 and 12 are the results of three source momentum conservation calculations. The calculations do not reproduce the data for $\theta_1 = -25^\circ$ as well as they do for $\theta_1 = -45^\circ$. Most noticeably the calculations predict a strong peak at small positive angles for p - p and d - d correlations in the C + C systems and for p - p correlations in the heavy systems. The general trends are, however, reproduced in most cases with the best agreement for d - d correlations in the heavy systems.

The peak at small positive angles for C + C systems comes from the very large contribution to the two-particle correlation function coming from the projectile-like source. This contribution is shown for the two-deuteron correlations in Fig. 10(c). For the C + Au system, the projectile-like source contribution at the most forward angles is still less than that of the intermediate source as shown in Fig. 9(c). For both the C + C and C + Au systems the importance of the target-like source is considerably less for $\theta_1 = -25^\circ$ than it is for $\theta_2 = -45^\circ$. The contribution to the two-deuteron coincidence cross section coming from the intermediate source is very similar for the two tag angles.

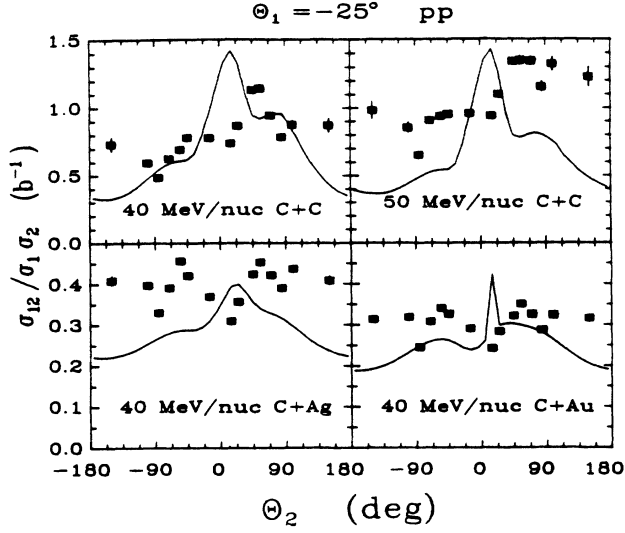


FIG. 11. Two-proton correlation function for which one proton is detected at $\theta_1 = -25^\circ$. The lines are the results of momentum conservation model calculations as described in the text.

F. Out-of-plane correlations

In addition to the in-plane correlations described in the previous sections, two-particle out-of-plane correlations were also measured. Correlations were measured between the out-of-plane tag telescopes ($\Phi = 90^\circ$) and the nine in-plane detectors with $\Phi = 0^\circ$. The correlations will first be presented in terms of the two-particle correlation function used in the previous section. Then the ratio of in-plane to out-of-plane correlations will be discussed.

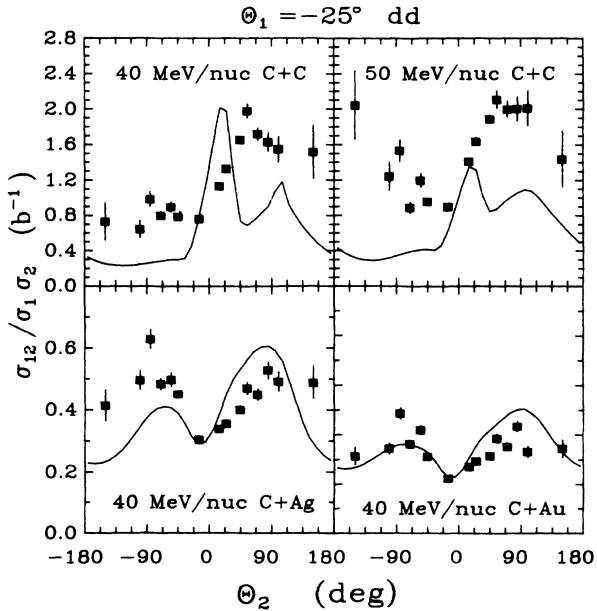


FIG. 12. Two-deuteron correlation function for which one deuteron is detected at $\theta_1 = -25^\circ$. The lines are the results of momentum conservation model calculations as described in the text.

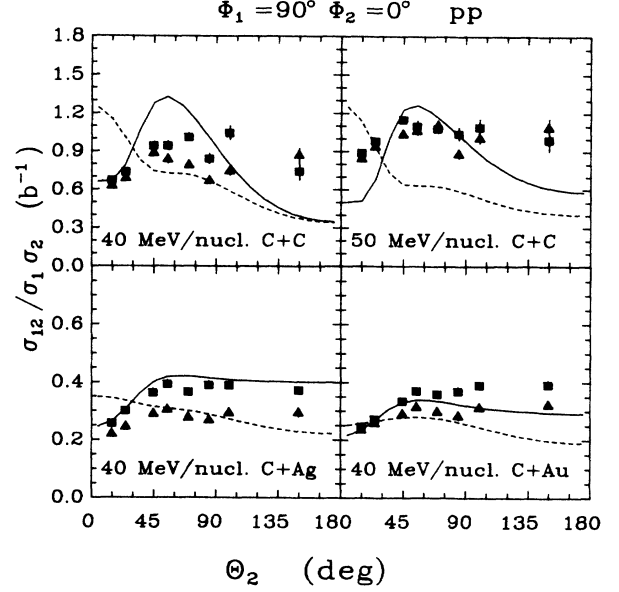


FIG. 13. Two-proton out-of-plane correlation function for $\theta_1 = 25^\circ$ (triangles and dashed lines) and $\theta_1 = 45^\circ$ (squares and solid lines). The lines are the results of momentum conservation model calculations as described in the text.

The two-particle out-of-plane correlation functions for p - p and d - d are shown in Figs. 13 and 14. The lines are the results of three-source momentum conservation calculations. One particle is detected at $\Phi = 90^\circ$ with $\theta_1 = 25^\circ$ (triangles and dashed lines) or 45° (squares and solid lines). The second particle is detected at $\Phi = 0^\circ$ with $15^\circ \leq \theta_2 \leq 150^\circ$. The correlations are integrated over the same energy ranges as the in-plane correlations. The correlation functions show very little difference between

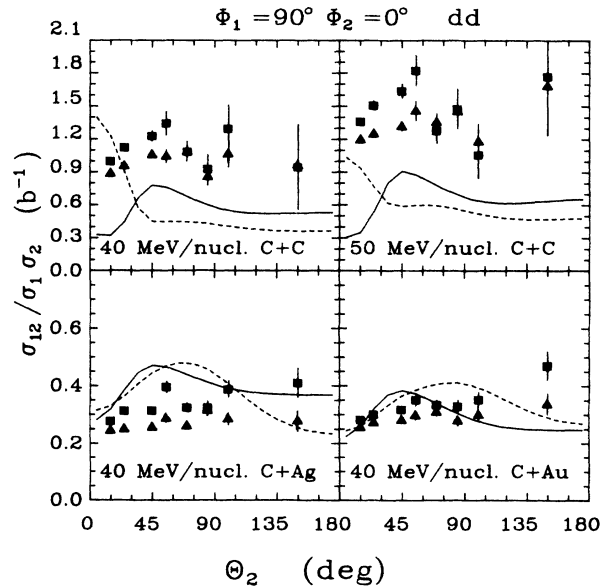


FIG. 14. Two-deuteron out-of-plane correlation function for $\theta_1 = 25^\circ$ (triangles and dashed lines) and $\theta_1 = 45^\circ$ (squares and solid lines). The lines are the results of momentum conservation model calculations as described in the text.

the different systems. The p - p and d - d correlations rise slowly from $\theta_2 = 15^\circ$ to 45° and then level off.

For the p - p correlations the momentum conservation calculations do an excellent job of reproducing the general trend and magnitude of the data for the heavy systems. In the $C + C$ system, the trend but not the magnitude of the correlations is reproduced for $\theta_1 = -45^\circ$. For $\theta_1 = -25^\circ$ the calculation has a large maximum at forward angles where the data has a minimum.

For the d - d correlations the calculation once again gets the trend but not the magnitude of the $C + C$ systems for $\theta_1 = -45^\circ$ and has a maximum at forward angles for $\theta_2 = -25^\circ$. In the heavier systems the general trend is reproduced by the calculations for both angles when one remembers that for large-angle correlations between deuterons emitted from the target source and those emitted from either the projectile or intermediate sources are not included in the calculation. These correlations between deuterons from different sources will raise the calculation at backward angles where the singles cross sections are dominated by the target-like source.

The ratio of in-plane to out-of-plane correlations for the tag detectors at θ_1 is defined as

$$R(\theta_2) = \frac{\sigma_{12}(\theta_1, \Phi_1 = 180^\circ, \theta_2, \Phi_2 = 0^\circ) / \sigma_1(\theta_1, \Phi_1 = 180^\circ)}{\sigma_{12}(\theta_1, \Phi_1 = 90^\circ, \theta_2, \Phi_2 = 0^\circ) / \sigma_1(\theta_1, \Phi_1 = 90^\circ)}, \quad (5)$$

where σ_{12} is the two-particle coincidence cross section for in-plane ($\Phi_1 = 180^\circ$) or out-of-plane ($\Phi_1 = 90^\circ$) and σ_1 is the singles cross section for the in-plane tag ($\Phi_1 = 180^\circ$) or the out-of-plane tag ($\Phi_1 = 90^\circ$). The ratio of in-plane to out-of-plane correlations are shown in Figs. 15–17 for the 45° tag telescopes. The lines are the results of three source momentum conservation calculations. The data show very little difference between the two $C + C$ systems and between the two heavier systems ($C + Ag$ and $C + Au$).

For the 45° tag telescopes the momentum conservation calculations do an excellent job of reproducing both the shape and magnitude for the heavy systems. For the $C + C$ systems the momentum conservation calculations over-predict the in-plane to out-of-plane ratio. The overprediction of the ratio for the $C + C$ systems is probably due to the greater importance of correlations between particles from different sources in the light systems than in the heavy systems. Correlations between particles coming from different sources would lower the ratio of in-plane to out-of-plane correlations. These results differ from our previous results.²⁷

Recently Bauer²⁸ has studied two-proton correlations using the Boltzmann-Uehling-Uhlenbeck (BUU) equation modified to conserve momentum. In the BUU approach the reaction being studied is simulated using 100 parallel ensembles of test particles. The test particles move in a mean field with collisions treated using a cascade approach with Pauli blocking. The results, shown in Fig. 18 for 40 MeV/nucleon $C + C \rightarrow pp$, reproduce the overall trend of the data. Bauer's BUU calculations have also reasonably reproduced the in-plane to out-of-plane ratio for 85 MeV/nucleon $C + C$ (Refs. 15 and 16) and the azimuthal correlations for 25 MeV/nucleon $O + C$.¹⁷

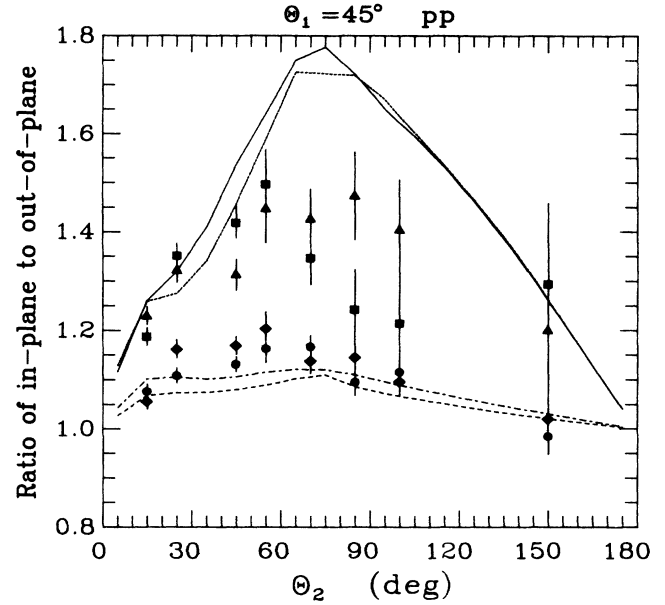


FIG. 15. Ratio of in-plane to out-of-plane correlations for two-protons for 40 MeV/nucleon $C + C$ (squares and solid lines), $C + Ag$ (circles and dashed-dotted lines), $C + Au$ (diamonds and dashed lines), and 50 MeV/nucleon $C + C$ (triangles and dotted lines). One proton is detected at $\theta_1 = 45^\circ$. The lines are results of momentum conservation model calculations as described in the text.

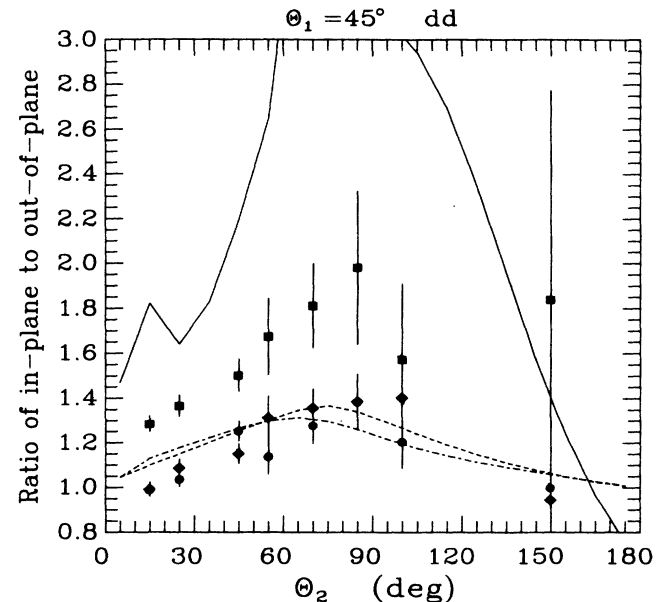


FIG. 16. Ratio of in-plane to out-of-plane correlations for two-deuterons for 40 MeV/nucleon $C + C$ (squares and solid lines), $C + Ag$ (circles and dashed-dotted lines), $C + Au$ (diamonds and dashed lines), and 50 MeV/nucleon $C + C$ (triangles and dotted lines). One proton is detected at $\theta_1 = 45^\circ$. The lines are results of momentum conservation model calculations as described in the text.

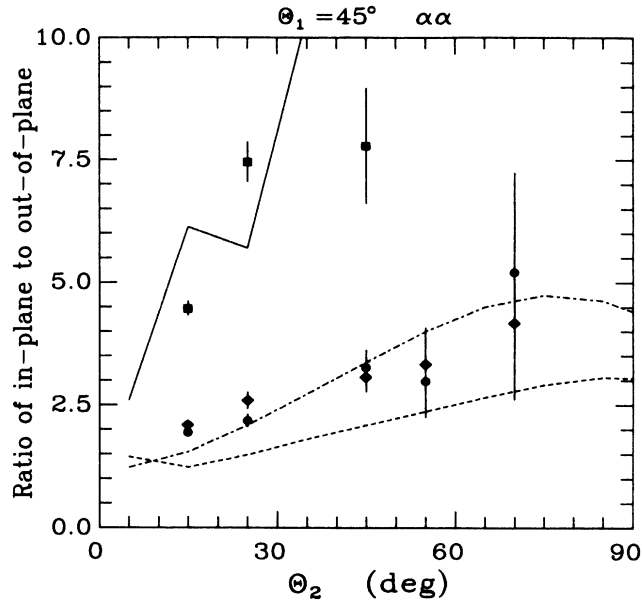


FIG. 17. Ratio of in-plane to out-of-plane correlations for two-alfas for 40 MeV/nucleon C + C (squares and solid lines), C + Ag (circles and dashed-dotted lines), C + Au (diamonds and dashed lines), and 50 MeV/nucleon C + C (triangles and dotted lines). One alpha is detected at $\theta_1 = 45^\circ$. The lines are results of momentum conservation model calculations as described in the text.

IV. UNSTABLE RESONANCES

A. Two-particle correlation functions

In this section the two-particle correlation functions at small-relative momentum will be presented. The correlation function, $R(\Delta p) + 1$, is defined as

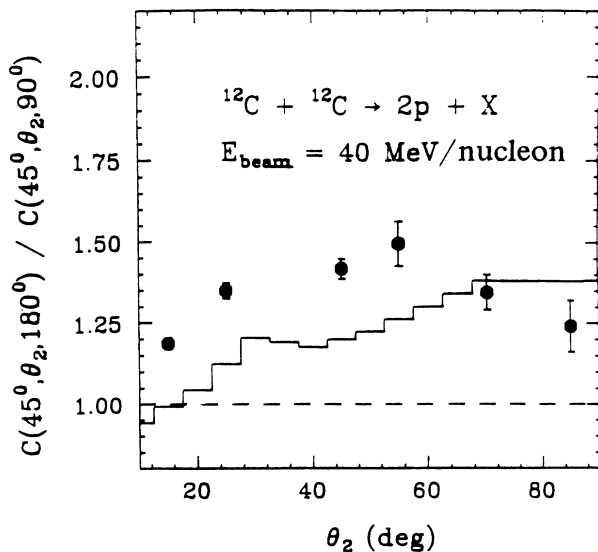


FIG. 18. Ratio of in-plane to out-of-plane correlations for two protons from 40 MeV/nucleon C + C using the BUU model (Ref. 28) (histogram) compared to the data (circles).

$$R(\Delta p) + 1 = N \sigma_{12}(\Delta p) / \sigma'_{12}(\Delta p), \quad (6)$$

where σ_{12} is the number of particle pairs with relative momentum Δp , σ'_{12} is the number of randomized particle pairs with relative momentum Δp , and N is a normalization constant picked such that the correlation function for large Δp is one. The random particle pairs are created by keeping the last five of each particle type and calculating their momentum relative to the current particle pair. Thus for each actual correlation, ten random correlations are generated.

The two-particle correlations are shown in Figs. 19–21. The lines in each figure are the results of calculations by Boal and Shillcock²⁹ for final state interactions between the emitted particles for various source radii coming from Coulomb and nuclear interactions between the two particles. For some of the particle pairs (p - t and d - t) the calculation has been carried out using the Coulomb interaction only. The calculations have been smeared to account for the experimental resolution of the MWPC and telescope array. Both the calculations and the smearing will be discussed in Sec. V.

The two-proton correlation function at small relative momentum is shown in Fig. 19. The correlation function has a broad maximum at $\Delta p = 20$ MeV/ c . The peak height decreases with increasing angle. This peak has been described previously in terms of both emission of ^2He (Ref. 30) and in-flight final state interactions between two randomly emitted protons.³¹ In Koonin's³¹ description the correlation function depends on the space-time extent of the emitting system and is often used to extract the source size of the emitting system. The extraction of source sizes from the correlation functions will be discussed later in greater detail. The correlation function also shows an anticorrelation for small Δp caused by Coulomb repulsion between the two protons. Calculations of the correlation function as a function of the size of the emitting source are shown in Fig. 19 for radius $r = 4.0$ (solid line), 4.5 (dotted line), 5.0 (dotted-dashed

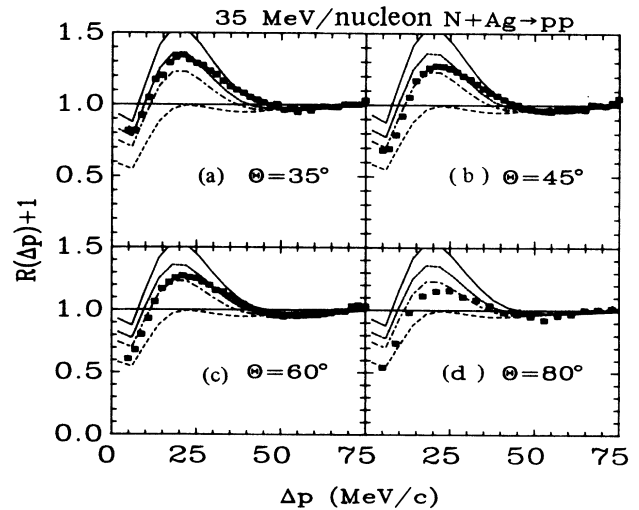


FIG. 19. Two-proton correlation function for 35 MeV nucleon N + Ag. The lines are the results of final-state interaction calculations as described in the text.

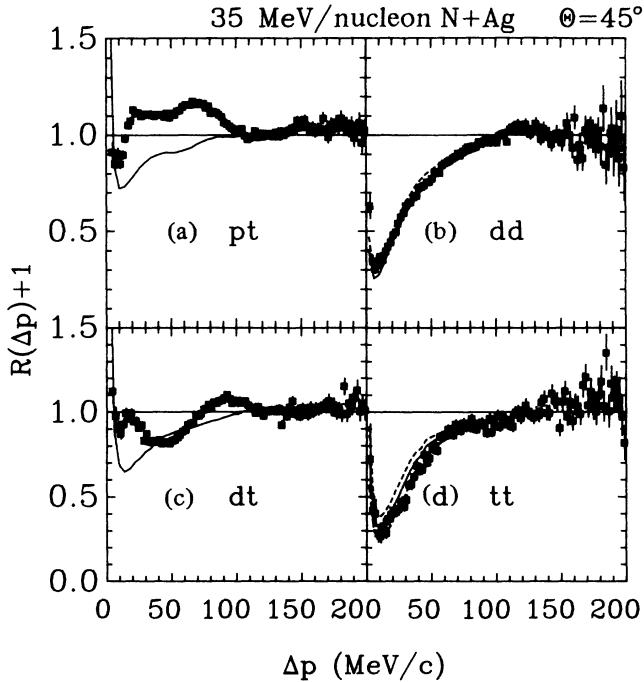


FIG. 20. Correlation functions for proton-triton, deuteron-deuteron, deuteron-triton, and triton-triton from 35 MeV/nucleon N + Ag at 35°.

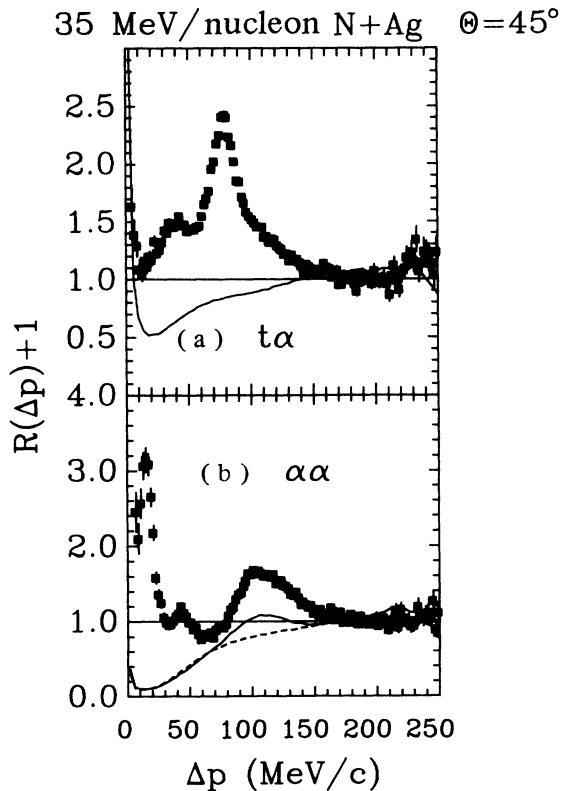


FIG. 21. Correlation functions for triton-alpha and alpha-alpha from 35 MeV/nucleon N + Ag at 45°.

line), and 7.0 fm (dashed line).

The proton-triton correlation function is shown in Fig. 20(a). The correlation function has a series of three unresolved peaks corresponding to the first three excited states ($E_{ex}=20.1, 21.1,$ and 22.1 MeV) in ${}^4\text{He}$ which can decay via proton or neutron emission. The solid line is the calculated correlation function for a source of radius 7.0 fm.

The two-deuteron correlation function is shown in Fig. 20(b). The two-deuteron correlation function rises smoothly to one. The calculated correlation function is shown for sources of radius 7.0 (solid line), and 8.0 fm (dashed line).

The deuteron-triton correlation function is shown in Fig. 20(c). The correlation function has two peaks corresponding to the second and third excited states ($E_{ex}=16.76$ and 19.8) in ${}^5\text{He}$.

The two-triton correlation function is shown in Fig. 20(d). Like the two-deuteron correlation function, the two-triton correlation function rises smoothly to one. The calculated correlation function is shown in Fig. 20(d) for sources of radius 6.0 (dotted-dashed line), 7.0 (solid line), and 8.0 fm (dashed line).

The triton-alpha correlation function is shown in Fig. 21(a). The large peak at $\Delta p=70$ MeV/c comes from the decay of the second excited state ($E_{ex}=4.630$ MeV) of ${}^7\text{Li}$. Lying at higher Δp are the next two states of ${}^7\text{Li}$ ($E_{ex}=6.68$ and 7.4597 MeV). The bump at $\Delta p=30$ MeV/c has been attributed by Pochodzalla *et al.*²⁴ to two step decays such as ${}^8\text{Li}^* \rightarrow t + {}^5\text{Li} \rightarrow t + \alpha + n$.

The two-alpha correlation function is shown in Fig. 21(b). The peak at $\Delta p=18$ MeV/c comes from the decay of the particle unstable ground state of ${}^8\text{Be}$. The broad peak at $\Delta p=110$ MeV/c corresponds to the first excited state ($E_{ex}=3.04$) of ${}^8\text{Be}$. The peak at $\Delta p=40$ MeV/c is the combination of the decay of the ${}^9\text{Be}_{2.43}^*$ state which decays by emitting an alpha leaving a ${}^5\text{Li}$ which in turn decays to a proton and an alpha,²⁴ and the ghost state of the ${}^8\text{Be}$ ground state.³²⁻³⁴ The calculated correlation function is shown in Fig. 21(b) for a source of radius 7.0 fm including the nuclear interaction (solid line) and for a Coulomb only interaction (dashed line).

B. Source sizes

Two-particle correlations have been used for some time to determine the size of the emitting source. In astronomy the Hanbury-Brown Twist interferometer is used to measure the size of stars by looking at two-photon correlations.³⁵ Two-pion correlations have been used in high-energy³⁶ and nuclear physics^{37,38} to measure the space-time extent of the interaction region. In nuclear physics two-proton correlations have been used to extract information about the space-time extent of the interaction region by many authors³⁹⁻⁴² using the description of Koonin.³¹ Recently, two-particle nuclear interferometry has been extended to other particle pairs by Boal and Shillcock.²⁹ Chitwood *et al.*²² and Pochodzalla *et al.*^{24,43} have used the calculations of Boal and Shillcock to extract source sizes from several particle pairs. In most cases the finite lifetime of the emitting source is neglected. The effect of neglecting the finite life-

TABLE VI. Extracted source radii (fm) from two-particle correlations 35 MeV/nucleon N + Ag.

Correlation	35°	45°	60°	80°	Average
<i>pp</i>	4.3±0.3	4.5±0.3	4.5±0.3	4.8±0.3	4.5±0.2
<i>pd</i>	9.3±0.8	9.1±0.7	9.6±0.8	10.2±0.9	9.5±0.4
<i>pα</i>	5.0±0.3	4.6±0.3	4.6±0.3	4.4±0.4	4.7±0.2
<i>dd</i>	6.7±0.8	7.3±0.7	8.8±0.9	7.6±1.0	7.5±0.4
<i>dα</i>	5.2±0.5	4.9±0.4	5.0±0.5	4.9±0.5	5.0±0.2
<i>tt</i>	6.6±1.1	5.9±0.8	6.4±1.2	7.1±2.1	6.3±0.5
<i>αα</i>	4.7±0.3	4.2±0.3	4.3±0.5		4.4±0.2

time of the emitting source is to increase the extracted source radius.

The source sizes have been extracted for *p-p*, *p-d*, *p-α*, *d-d*, *d-α*, *t-t*, and *α-α* correlations by using the calculations of Boal and Shillcock smeared for the experimental resolution. The smearing was done by taking the calculated correlation function and multiplying by the random correlations, $\sigma'_{12}(\Delta p)$, to produce σ_{12} . The resulting σ_{12} was then smeared assuming a Gaussian shaped distribution of width δp . For the correlations with resonances the width, δp , was adjusted so that the full width at half maximum (FWHM) of the smeared correlation function was the same as the FWHM of the peak in the data. For the correlations without resonances the width was adjusted to give a shape as similar to the data as possible. The smeared calculations are shown in Figs. 19–21 as lines.

The source radii were determined by χ^2 minimization at each angle for each particle pair. The extracted radii, given in Table VI, are in general agreement with previous results.^{22,24,43} The extracted radii show little variation with angle or beam energy. The radius extracted from the *d-α* correlations are larger by about 1 fm than those obtained previously.^{22,24} This difference is probably due to the resolution in the present experiment.

One interesting feature of the extracted radii is that for those correlations involving particle pairs that do not have resonances (*p-d*, *d-d*, and *t-t*), the size of the emitting source is larger than for those pairs that have resonances. This pattern has been seen before.^{22,24,43} Chitwood *et al.*²² also found that the source radii extracted from the first peak in the *d-α* correlations was smaller by about 0.5 fm from the radii extracted from the second peak. The calculations by Boal²⁹ assume that all the two-particle correlations come from particles that are randomly emitted and then have in-flight final state interactions. For randomly emitted particles experiencing

in-flight final state interactions one would expect that a single source size would describe all the states. If, however, some of the observed correlations come instead from the decay of emitted particle unstable nuclei, then the extracted source radius would be smaller than the true radius and since the different states are populated according to the temperature of the system, it is possible that different states will yield different apparent source radii.

It has been suggested that the different extracted source radii may result from a sequential freeze-out.^{29,44} In the case of sequential freeze-out, different particles may be used to probe different stages of the interaction.

The source radii extracted using two-particle correlations at small relative momentum can also be compared to the radius extracted using the coalescence model.^{8,45,46} For 92 and 137 MeV/nucleon Ar + Ca, Au reactions⁸ the source radius extracted using the coalescence model for particles of mass 2–14 was $r=3.7$ fm. This radius is slightly smaller than the radius extracted from *pp* and *αα* correlations and much smaller than the radius extracted from *pd*, *dd*, and *tt* correlations (6–10 fm). It should be remembered that the extraction of the source radius from the two-particle correlations was done neglecting the lifetime of the emitting system. If one includes the finite lifetime of the emitting system then the measured source radius will decrease.

C. Bound state spectra

The single-particle inclusive energy spectra for the bound states of He, Li, Be, and B are shown in Fig. 22 (see also Table VII). The lines are the result of single moving source fits to $\theta=45^\circ$, 60° , and 80° . The extracted source parameters are listed in Table VII along with the Coulomb shifts used in the fits. The fits indicate that the intermediate velocity source dominates the cross sections

TABLE VII. Moving source parameters for 35 MeV/nucleon N + Ag.

Particle	V_c (MeV)	Cross section (mb)	Velocity (c)	Temperature (MeV)
³ He	8	223±15	0.162±0.011	12.4±0.5
⁴ He	8	2090±100	0.095±0.003	12.1±0.4
⁶ He	8	55±5	0.072±0.004	14.2±0.5
⁶ Li	12	66±4	0.116±0.003	15.1±0.3
⁷ Li	12	119±7	0.108±0.004	14.6±0.3
⁷ Be	16	35±3	0.128±0.003	14.6±0.3
^{9,10} Be	16	40±3	0.115±0.002	15.2±0.3
B	20	140±50	0.122±0.004	13.4±0.6

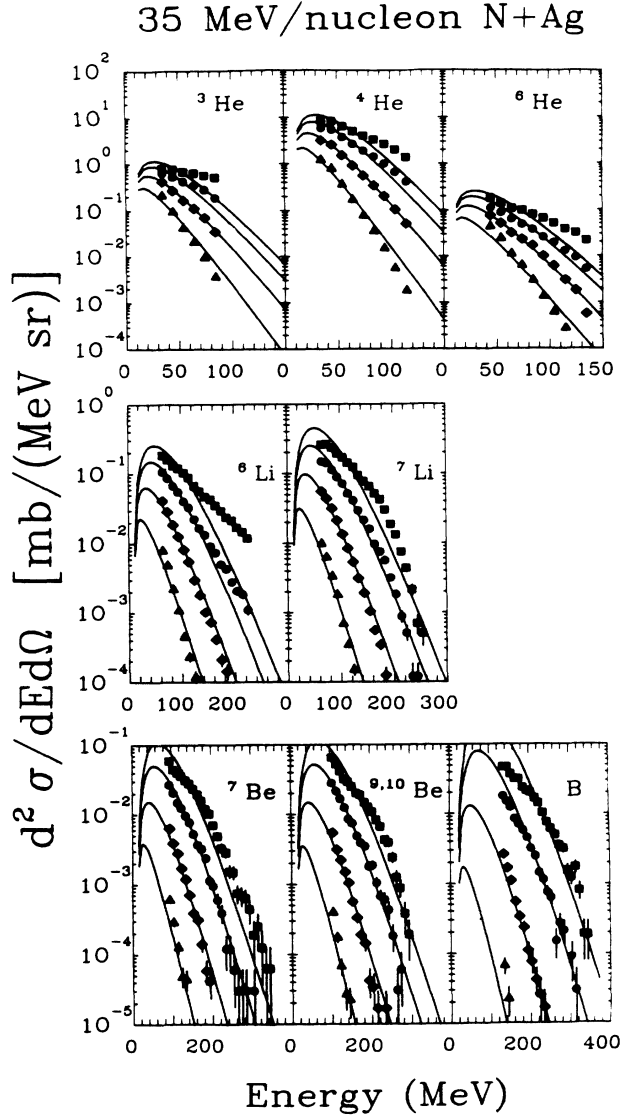


FIG. 22. He, Li, Be, and B energy spectra for 35 MeV/nucleon N + Ag. The lines are moving source fits as described in the text.

for $\theta=45^\circ-80^\circ$. The 35° spectra show signs of enhancement due to contributions from the projectile-like source. The extent of contamination of the ${}^7\text{Li}$ spectra by the decay of ${}^8\text{Be}$ (Ref. 45) is estimated to be 4.3 mb of ${}^8\text{Be}$ identified as ${}^7\text{Li}$ per 50 mb of ${}^8\text{Be}$. Based on the cross sections for the stable Be isotopes this means that about 2–4 mb of the ${}^7\text{Li}$ cross section comes from the decay of ${}^8\text{Be}$.

D. Populations of particle unstable states

In order to extract the populations of particle unstable states, the contribution to the two-particle correlation functions coming from randomly emitted particles must be subtracted. The populations of particle unstable states were found by integrating the two-particle coincidence cross section $\sigma_{12}(\Delta p)$ over those values of Δp that correspond to the state of interest. For each Δp step the cross section is given by

$$\sigma = \{ \sigma_{12}(\Delta p) - \sigma'_{12}(\Delta p) [R(\Delta p) + 1] / N \} / \epsilon(\Delta p), \quad (7)$$

where $\sigma_{12}(\Delta p)$, $\sigma'_{12}(\Delta p)$, and N are the same as before (Sec. IV A). $R(\Delta p) + 1$ is the theoretical correlation function for Coulomb only final state interactions for a source radius r , and $\epsilon(\Delta p)$ is the efficiency of the MWPC-phoswich array calculated by a Monte Carlo calculation. The cross sections were extracted using source radii of $r=7$ and 8 fm for the theoretical correlation function, $R(\Delta p) + 1$. The extracted cross sections given in Table VIII are for a source size of $r=7$ fm with errors including the uncertainty arising from the use of a different source size, a 10% uncertainty for the efficiency calculation, and statistics.

The extraction of the populations of the particle unstable states was done assuming that randomly emitted particles have Coulomb only final-state interactions. Two-particle correlations coming from randomly emitted particles which interact through nuclear forces to produce resonant states are indistinguishable from emitted particle unstable states. Possible corrections for these random correlations will be discussed in Sec. IV F.

TABLE VIII. Extracted cross sections of particle unstable states (mb/sr).

State(s)	35 MeV/nucleon			
	35°	45°	60°	80°
${}^4\text{He}_{20,21,22}^*$	3.5 ± 0.6	1.11 ± 0.16	0.24 ± 0.04	0.043 ± 0.007
${}^5\text{He}_{16,76}^*$	0.39 ± 0.18	0.14 ± 0.08	0.042 ± 0.015	0.008 ± 0.003
${}^5\text{He}_{19,8}^*$	0.75 ± 0.24	0.44 ± 0.08	0.081 ± 0.018	0.010 ± 0.003
${}^5\text{Li}_{g.s.,7,5}$	11.5 ± 10.6	2.7 ± 0.3	0.42 ± 0.05	0.031 ± 0.005
${}^6\text{Li}_{2,186}^*$	11.3 ± 10.4	2.7 ± 0.3	0.46 ± 0.06	0.031 ± 0.004
${}^6\text{Li}_{4,31,5,65}^*$	1.56 ± 0.29	0.34 ± 0.06	0.058 ± 0.010	0.0027 ± 0.0008
${}^7\text{Li}_{4,63}^*$	7.2 ± 0.9	1.05 ± 0.13	0.151 ± 0.019	0.0074 ± 0.0012
${}^7\text{Li}_{6,68,7,46}^*$	3.2 ± 0.5	0.44 ± 0.06	0.043 ± 0.008	0.0011 ± 0.0005
${}^8\text{Be}_{3,04}^*$	3.77 ± 0.03	0.399 ± 0.004	0.0503 ± 0.011	

E. Quantum statistical model and extraction of nuclear temperature

Previous work has established the importance of feeding of light nuclei by the decay of heavier particle unbound states.^{21,24,48} In order to extract information such as temperature from the relative populations of states, the amount of feeding to each individual state needs to be measured or calculated. Using the quantum statistical model of Hahn and Stöcker⁴⁹ the extent of feeding to each of the observed states may be calculated. In the quantum statistical model the initial population of a state is determined from its chemical potential, statistical weight and the temperature. Approximately 40 stable and 500 unstable nuclear levels up to mass 20 are included in the calculation. After the initial populations are determined, the excited states are allowed to decay using the known branching ratios.

We have extracted the nuclear temperature for the 35 MeV/nucleon system by χ^2 minimization using the quantum statistical model. For the quantum statistical model calculation the neutron to proton ratio was calculated using the fireball model^{1,2} and was found to be 19/17 for the most probable impact parameter. The break-up density was fixed at $\rho=0.18\rho_0$, which is the density obtained from a break-up radius of 7 fm and a source of 36 nucleons. The temperature was extracted using the populations of the particle bound states measured in the singles run and the particle unstable states extracted from the two-particle correlations. In addition, the data of Morrissey^{18,19} and Bloch^{25,47,50} for γ - and neutron-emitting states for the same system were also included. For the particle bound states the ratio of the cross section each for isotope extracted from the moving source fit to the ${}^6\text{Li}$ ground-state cross section was compared to the ratio calculated by the quantum statistical model. For the particle unstable states the cross sections given in Table VIII were integrated from $\theta=45^\circ$ to 80° , which corresponds to $\theta=35^\circ-90^\circ$ due to the 20° opening angle of the MWPC-phoswich array. The 35° data have been excluded because they contain a component coming from the projectile-like source. The ratio of these integrated cross sections were then taken to the cross section of either the ground state of the appropriate isotope or to ${}^6\text{Li}$ ground state integrated over the same angles and energies using the moving source parameters. These ratios are given in Table IX, the quoted errors include a 10% uncertainty in the absolute normalizations for the particle unstable states and the particle bound states. Using these parameters the temperature was determined to be $4.8^{+2.8}_{-2.4}$ MeV. In Fig. 23 the calculated ratios for temperatures of $T=4.8$ and 14 MeV are compared to the data. The moving source fits to the bound state kinetic energy spectra indicate a source temperature of about 14 MeV. The 14 MeV calculation shown in Fig. 23 clearly does a very poor job of fitting the data. The extracted temperature of 4.8 MeV agrees with the temperature extracted at higher-energies (60 MeV/nucleon Ar + Au) (Ref. 24) using the quantum statistical model, and with the temperatures extracted from widely separated states in ${}^5\text{Li}$ for 35 MeV/nucleon N + Au (Ref. 23) and ${}^5\text{Li}$ and ${}^8\text{Be}$ for 60

TABLE IX. Excited-state ratios for 35 MeV/nucleon N + Ag.

State	Ratio to	Ratio
${}^4\text{He}_{20,1,21,1,22,1}^*$	${}^4\text{He}_{g.s.}$	$0.013^{+0.006}_{-0.005}$
${}^5\text{He}_{16,76}^*$	${}^6\text{Li}_{g.s.}$	$0.015^{+0.015}_{-0.009}$
${}^5\text{He}_{19,8}^*$	${}^6\text{Li}_{g.s.}$	$0.048^{+0.024}_{-0.018}$
${}^5\text{Li}_{g.s.,5}$	${}^6\text{Li}_{g.s.}$	$0.77^{+0.35}_{-0.25}$
${}^6\text{Li}_{2,186}^*$	${}^6\text{Li}_{g.s.}$	$0.60^{+0.27}_{-0.20}$
${}^6\text{Li}_{4,31,5,65}^*$	${}^6\text{Li}_{g.s.}$	$0.074^{+0.038}_{-0.027}$
${}^7\text{Li}_{4,65}^*$	${}^7\text{Li}_{g.s.}$	$0.20^{+0.09}_{-0.06}$
${}^7\text{Li}_{6,68,7,456}^*$	${}^7\text{Li}_{g.s.}$	$0.078^{+0.037}_{-0.027}$
${}^8\text{Be}_{3,04}^*$	${}^6\text{Li}_{g.s.}$	$0.17^{+0.08}_{-0.06}$

MeV/nucleon Ar + Au (Ref. 24).

To illustrate the importance of feeding, Fig. 24 shows the calculated feeding for several states. In general, over half the observed bound state spectra come from the decay of heavier states. Two of the particle unstable states (${}^7\text{Li}_{0,476}^*$ and ${}^8\text{Be}_{3,04}^*$) are heavily fed, but most of the particle unstable states are affected very little by feeding from higher states.

The difference between the temperature extracted from the kinetic energy spectra and the population of the states may be related to time of formation of the complex fragments. The kinetic energy spectra of the protons and neutrons in the intermediate source are fixed in the early hot stage of the interaction. If complex fragments are formed later as the source is cooling, then the distributions of the states will reflect the later cooler temperature. The kinetic energy spectra of the complex fragments are determined by the spectra of the protons and neutrons that coalesced to form the fragment.

Similarly, it has been pointed out that while the average energy per particle stays constant during the expansion of the source, the relative abundances of the states change as the source expands and cools.²⁹ Thus the ki-

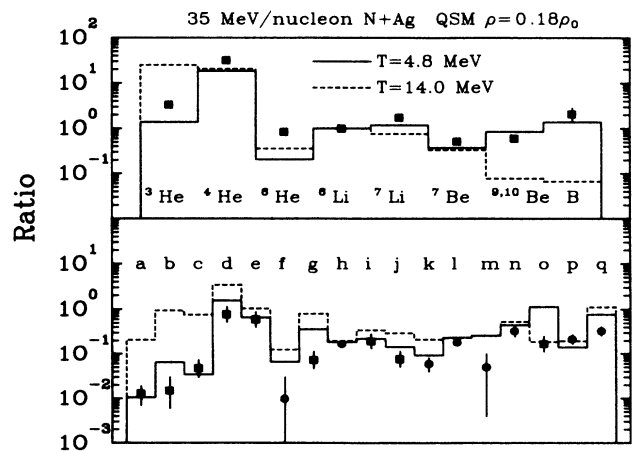


FIG. 23. Quantum statistical model calculations of the production of the measured state for $T=4.8$ and 14.0 MeV and $\rho=0.18\rho_0$. The excited states and particle unbound states shown in the bottom half of the figure are identified in Table X.

TABLE X. Key to particle unstable and gamma states in Fig. 23.

Letter	State	Decay	Reference
a	${}^4\text{He}_{20,1,21,1,22,1}^*$	$p-t$	
b	${}^5\text{He}_{16,7}^*$	$d-t$	
c	${}^5\text{He}_{19,7}^*$	$d-t$	
d	${}^5\text{Li}_{g.s.,7,5}^*$	$p-\alpha$	
e	${}^6\text{Li}_{2,186}^*$	$d-\alpha$	
f	${}^6\text{Li}_{3,6}^*$	γ	18
g	${}^6\text{Li}_{4,35,5,65}^*$	$d-\alpha$	
h	${}^7\text{Li}_{0,476}^*$	γ	47
i	${}^7\text{Li}_{4,65}^*$	$t-\alpha$	
j	${}^7\text{Li}_{6,68,7,456}^*$	$t-\alpha$	
k	${}^7\text{Li}_{7,456}^*$	$n-{}^6\text{Li}$	25
l	${}^7\text{Be}_{0,430}^*$	γ	47
m	${}^8\text{Li}_{0,98}^*$	γ	19
n	${}^8\text{Li}_{2,255}^*$	$n-{}^7\text{Li}$	25
o	${}^8\text{Be}_{3,04}^*$	$\alpha-\alpha$	
p	${}^{10}\text{Be}_{7,371}^*$	$n-{}^9\text{Be}$	50
q	${}^{12}\text{B}_{3,388}^*$	$n-{}^{11}\text{B}$	50

netic energy spectra will reflect the temperature of the early hot stage of the interaction, while the populations of different states will reflect the temperature at the time of freeze-out. If this is the case, then freeze-out appears to occur at a temperature of around 5 MeV for interactions in the 35–60 MeV/nucleon range.

F. Final-state interactions versus emission of particle unstable nuclei

One of the most important questions that arises in the measurement of the nuclear temperature through the measurement of particle unstable states is the question of

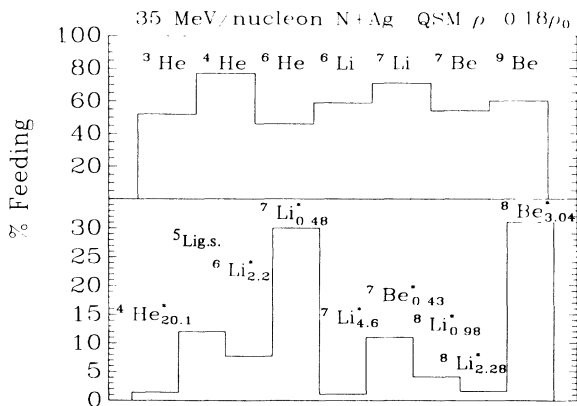


FIG. 24. Quantum statistical model calculation of the feeding to the observed states for a source temperature of 4.8 MeV and a freeze-out density of $0.18\rho_0$.

at what point does one consider a particle to have been formed and emitted. In particular, is the emission of particle unstable nuclei the same as in-flight final-state interactions or is it a totally different process? If the latter is the case, then one is only interested in those two-particle correlations that come from the decay of emitted unstable nuclei when extracting the temperature of the emitting source. The problem then arises of how to eliminate the in-flight final-state interactions from the observed two-particle correlations. This could be accomplished if one could determine a unique source size for all particles. One would then be able to use the calculated correlation function for the nuclear and Coulomb final-state interactions in the extraction of the populations of the particle unstable states.

The problem of determining whether final state interactions are the same as emission of particle unstable nuclei can be examined by looking at the trends shown in the two-particle correlations. As mentioned earlier, correlations involving two particles that exhibit resonances have a consistently smaller extracted source radii than those particle pairs with no resonances. It has been suggested that differences in the time of freeze-out for different particles may be responsible for these different radii.²⁹ On the other hand if all particles come from a source that is the same size and if the emission of particle unstable nuclei and final-state interactions are different processes, then correlations involving particles with resonances will be enhanced and a smaller source radii will be extracted for these correlations. In addition, the difference between the extracted source radii for the two peaks in the $d-\alpha$ correlations²² could then be understood in terms of a greater enhancement of the lower-lying state leading to a smaller apparent radius for it.

It is also interesting to look at the behavior of two-proton correlations as a function of the size of the target nucleus. Two-proton correlations at small relative momentum have been studied for 25 MeV/nucleon ${}^{16}\text{O}+{}^{12}\text{C}$, ${}^{27}\text{Al}^{30}$, and ${}^{197}\text{Au}^{40}$. The peak of the correlation function increases with increasing target size. Using Koonin's model,³¹ this leads to a smaller extracted source radius as one increases the target size. If, on the other hand, one interprets the data in terms of the decay of ${}^2\text{He}$ then the data may be explained in terms of the ${}^2\text{He}$ cross section increasing with increasing source size.

The two-particle correlations have been observed to be stronger for higher two-particle total energy,^{22,24,43} leading to a smaller extracted source radius. It has been suggested that this may mean that higher-energy particles tend to come from smaller sources.²⁴ On the other hand, in the case of correlations with resonances this increase in observed correlations might be due to a greater cross section for the emission of particle unstable nuclei at high energy than the random emission of two lighter nuclei each at relatively high energies.

In the large-angle correlations presented earlier it was shown that the decay of particle unstable nuclei contribute heavily to the two-particle correlation function at relatively large angles ($10^\circ-25^\circ$). For the system nearest 35 MeV/nucleon $\text{N} + \text{Ag}$, 40 MeV/nucleon $\text{C} + \text{Ag}$, the large-angle correlations shown in Fig. 8 indicate that

there are about twice as many α - α coincidences on the same side of the beam as on opposite sides of the beam. In p - d and d - d correlations it was shown that there is a slight favoring of the opposite side over the same side for this system. The excess in same side correlations seen in Fig. 8 clearly must come from the emission of ${}^8\text{Be}$ and not from two alphas that have final state interactions.

Using Boal's²⁹ calculations of the final-state interaction including both the nuclear and Coulomb potentials for a radius of 7.0 fm the cross section for the first excited state of ${}^8\text{Be}$ was extracted in the same fashion as described in Sec. IV D. The cross section was found to be 0.507 ± 0.093 mb compared to 0.690 ± 0.097 mb obtained from the Coulomb only calculation. In addition to being smaller by about 25%, the cross section is now much more sensitive to the source radius that is used. Unfortunately the full nuclear and Coulomb calculation exists for only a limited number of the two-particle correlations that have resonances. In addition, in the present experiment the resolution is sufficient to perform the nuclear plus Coulomb background subtraction for the p - p and α - α cases only. The effect of subtracting a background that assumes a component coming from in-flight final-state interactions would be to lower the extracted cross sections of particle unstable states and hence reduce the extracted temperatures.

V. SUMMARY AND CONCLUSIONS

Single-particle inclusive kinetic energy spectra and two-particle large-angle correlation functions have been measured for 40 and 50 MeV/nucleon C induced reactions. The light-particle energy spectra have been well fit with a three moving source parametrization assuming the emission of particles from three distinct sources all moving in the beam direction. One source, the projectile-like source, has a velocity of about 85% of the incident beam velocity and a temperature of about 4–5 MeV. The second source, the target-like source, has a velocity of about 5–10% of the incident beam velocity with a temperature of 3.5–4.5 MeV. The spectra are dominated by the third source, the intermediate velocity source, which has a velocity intermediate between the projectile and target velocities and a temperature of 10–15 MeV.

Two-particle in-plane correlations were measured with tag detectors at $\theta_1 = -25^\circ$ and -45° . For both tag angles the C + C systems showed a strong preference for emission of two particles to opposite sides of the beam. The enhancement in opposite side emission increases as the total mass of the observed particles increases. Very little difference was observed between the two beam energies, 40 and 50 MeV/nucleon. For the heavier systems, C + Ag and C + Au, the correlations were more symmetric about the beam axis with opposite side correlations only slightly enhanced over same side correlations. For all four systems the decay of particle unstable light nuclei contributed heavily to the two-particle large-angle correlations. For an opening angle of 10° , enhancements in the correlation function are observed for p - p , p - t , p - ${}^4\text{He}$, d - ${}^4\text{He}$, t - ${}^4\text{He}$, and ${}^4\text{He}$ - ${}^4\text{He}$. The contribution to the correlation function for particle unstable resonances can

be as high as 80% (d - ${}^4\text{He}$ for 40 MeV/nucleon C + C). Out of plane correlations were also measured with tag telescopes at $\theta_1 = 25^\circ$ and 45° at $\Phi = 90^\circ$. The correlations were found to be nearly flat with a slight decrease at more forward angles. The ratio of in-plane to out-of-plane correlations shows an enhancement in the emission of particles in the same plane. As with the in-plane correlations, the enhancement is largest for the light systems and for higher total mass of the observed particles.

In order to determine the extent to which conservation of momentum affects the measured correlations, momentum conservation calculations were carried out. Using a momentum conservation calculation incorporating emission from all three sources, the general trend of the in-plane 45° tag correlations were reproduced. The overall agreement was not as good for the correlations with the 25° tag, perhaps due to the increased importance of correlations involving particles from different sources. For the out-of-plane correlations the agreement between the momentum conservation calculations and the data was good only for the heavier systems. The momentum conservation calculation did a reasonably good job of explaining the ratio of in-plane to out-of-plane correlations for the heavy systems. For the light systems the calculation consistently overpredicted the ratio of in-plane to out-of-plane correlations, this may in part be due to correlations between two particles from different sources.

A close packed array of sixteen phoswich telescopes positioned behind a multiwire proportional counter was used to measure two-particle correlations at small relative momentum for the reaction 35 MeV/nucleon N + Ag. The correlations were measured at central angles of $\theta = 35^\circ$, 45° , 60° , and 80° . The correlations have been used to extract information about the space-time extent and temperature of the intermediate velocity source. Source radii extracted from two-particle correlations are in good agreement with the radii extracted by previous authors. The radii are smallest for particle pairs with resonances, pp , $p\alpha$, $d\alpha$, and $\alpha\alpha$ (4.5–5.0 fm), and largest for nonresonant pairs, pd , dd , and tt (6.3–9.5 fm). Little difference was found in the extracted source radii as a function of angle and beam energy. The radii are somewhat larger than those extracted using the coalescence model due, in part, to the neglecting of the lifetime of the emitting source. If a nonzero source lifetime is used then smaller source radii are obtained.

One important question that has come up is when is a particle considered to have been emitted from the source? In particular, are particle unstable nuclei emitted from the source or are all observed resonances the results of in-flight final-state interactions? If particle unstable nuclei are emitted, in addition to other particles experiencing in-flight final state interactions, then the observed two-particle correlations are the results of a combination of the two processes. If this is the case, then radii extracted from particle pairs with resonances will be smaller than radii extracted from nonresonant pairs because the decay of particle unstable light nuclei will enhance the correlation functions which leads to a larger extracted radius. If, on the other hand, all observed resonances are the results of in-flight final-state interactions then the

differences in the extracted radii may indicate different emission times for different particles or perhaps that different particle pairs come from different types of collisions.

The difference between the source radii extracted using particle pairs with resonances and those without resonances has also been attributed to different freeze-out times for different particles. Those particles that freeze-out earlier will yield a smaller source radius than particles that freeze-out at a later stage of the interaction. In this view information about the source at different times may be obtained by looking at different particles.

Using the populations of bound and unbound states measured in the present experiment and the γ and neutron emitting states measured by Morrissey *et al.* and Bloch *et al.* a source temperature of $4.8^{+2.8}_{-2.4}$ MeV has been extracted. The quantum statistical model of Hahn and Stöcker was used in order to correct for feeding from higher-lying states to the observed states. Overall, the quantum statistical model does an excellent job of fitting the populations of all the measured states at the same time. The use of the quantum statistical model to take into account feeding from higher-lying states has eliminated the previous discrepancy in the temperature between measurements using particle bound γ -ray emitting states and measurements using particle unbound states. The temperature is in good agreement with the temperature extracted from particle unbound states for 35 MeV/nucleon N + Au and 60 MeV/nucleon Ar + Au. The temperature extracted from the population of states is about 10 MeV lower than the temperature extracted from the kinetic energy spectra. The reason for this disagreement may be that the two temperature measurements represent the temperature of the emitting source at different times. The kinetic energy spectra are fixed early in the interaction while the populations of the states

change as the source expands and cools. Thus the temperature measured from the populations of the states would represent the temperature at the time of freeze-out. If this is the case, then the freeze-out temperature does not change measurably for beam energies between 35 and 60 MeV/nucleon.

In conclusion it has been shown that two-particle large-angle correlations are consistent with emission from a thermally equilibrated system. While the measured two-particle correlations are not isotropic, as emission from a thermally equilibrated source would require, the effects of momentum conservation requirements have been shown to account for most of the deviation from an isotropic distribution. As the number of nucleons in the emitting source increases the correlation functions become more isotropic.

The use of the quantum statistical model has resolved the discrepancy between temperature measurements using the populations of γ -ray emitting states and those using particle unstable states. The temperature extracted from the populations of nuclear states is still considerably lower than the temperature extracted from the kinetic energy spectra. Further work is needed to eliminate the contribution of final state interactions to the populations of the particle unstable states. Theoretical calculations are needed for the nuclear final state interactions of several particle pairs and either a theoretical or experimental value for the freeze out radius is needed.

ACKNOWLEDGMENTS

The authors thank David Boal for providing the calculations of the correlation function based on Ref. 29. This work was supported by the National Science Foundation under Grant No. PHY-86-11210.

¹G. D. Westfall, J. Gosset, P. J. Johansen, A. M. Poskanzer, W. G. Meyer, H. H. Gutbrod, A. Sandoval, and R. Stock, *Phys. Rev. Lett.* **37**, 1202 (1976).
²J. Gosset, H. H. Gutbrod, W. G. Meyer, A. M. Poskanzer, A. Sandoval, R. Stock, and G. D. Westfall, *Phys. Rev. C* **16**, 629 (1977).
³H. H. Gutbrod, A. Sandoval, P. J. Johansen, A. M. Poskanzer, J. Gosset, W. G. Meyer, G. D. Westfall, and R. Stock, *Phys. Rev. Lett.* **37**, 667 (1976).
⁴G. D. Westfall, B. V. Jacak, N. Anantaraman, M. V. Curtin, G. M. Crawley, C. K. Gelbke, B. Hasselquist, W. G. Lynch, D. K. Scott, M. B. Tsang, M. J. Murphy, T. J. M. Symons, R. Legrain, and T. J. Majors, *Phys. Lett.* **116B**, 118 (1982).
⁵B. V. Jacak, G. D. Westfall, C. K. Gelbke, L. H. Harwood, W. G. Lynch, D. K. Scott, H. Stöcker, M. B. Tsang, and T. J. M. Symons, *Phys. Rev. Lett.* **51**, 1846 (1983).
⁶G. D. Westfall, Z. M. Koenig, B. V. Jacak, L. H. Harwood, G. M. Crawley, M. W. Curtin, C. K. Gelbke, B. Hasselquist, W. G. Lynch, A. D. Panagiotou, D. K. Scott, H. Stöcker, and M. B. Tsang, *Phys. Rev. C* **29**, 861 (1984).
⁷T. C. Awes, S. Saini, G. Poggi, C. K. Gelbke, D. Cha, R. Legrain, and G. D. Westfall, *Phys. Rev. C* **25**, 2361 (1982).

⁸B. V. Jacak, D. Fox, and G. D. Westfall, *Phys. Rev. C* **31**, 704 (1985).
⁹B. E. Hasselquist, G. M. Crawley, B. V. Jacak, Z. M. Koenig, G. D. Westfall, J. E. Yurkon, R. S. Tickle, J. P. Dufour, and T. J. M. Symons, *Phys. Rev. C* **32**, 145 (1985).
¹⁰S. Nagamiya, L. Anderson, W. Bruckner, O. Chamberlain, M.-C. Lemaire, S. Schnetzer, G. Shapiro, H. Steiner, and I. Tanihata, *Phys. Lett.* **81B**, 147 (1979).
¹¹I. Tanihata, M.-C. Lemaire, S. Nagamiya, and S. Schnetzer, *Phys. Lett.* **97B**, 363 (1980).
¹²I. Tanihata, S. Nagamiya, S. Schnetzer, and H. Steiner, *Phys. Lett.* **100B**, 121 (1981).
¹³W. G. Lynch, L. W. Richardson, M. B. Tsang, R. E. Ellis, C. K. Gelbke, and R. E. Warner, *Phys. Lett.* **108B**, 274 (1982).
¹⁴M. B. Tsang, W. G. Lynch, C. B. Chitwood, D. Fields, D. R. Klesch, C. K. Gelbke, G. R. Young, T. C. Awes, R. L. Ferguson, F. E. Obenshain, F. Plasil, and P. L. Robinson, *Phys. Lett.* **148B**, 265 (1984).
¹⁵P. Kristiansson, L. Carlen, H.-Å. Gustafsson, B. Jakobsson, A. Oskarsson, H. Ryde, J. P. Bondorf, O.-B. Nielsen, G. Lovhoiden, T.-F. Thorsteinsen, D. Heuer, and H. Nifenecker, *Phys. Lett.* **155B**, 31 (1985).

- ¹⁶P. Kristiansson, J. P. Bondorf, L. Carlen, H.-Å. Gustafsson, B. Jakobsson, A. Kristiansson, G. Lovhoiden, H. Nifenecker, O-B. Nielson, A. Oskarsson, H. Ryde, T-F. Thorsteinsen, and M. Westenius, *Nucl. Phys.* **A447**, 557c (1985).
- ¹⁷C. B. Chitwood, D. J. Fields, C. K. Gelbke, D. R. Klesch, W. G. Lynch, M. B. Tsang, T. C. Awes, R. L. Ferguson, F. E. Obenshain, F. Plasil, R. L. Robinson, and G. R. Young, *Phys. Rev. C* **34**, 858 (1986).
- ¹⁸D. J. Morrissey, W. Benenson, E. Kashy, B. Sherrill, A. D. Panagiotou, R. A. Blue, R. M. Ronningen, J. van der Plicht, and H. Utsunomiya, *Phys. Lett.* **148B**, 423 (1984).
- ¹⁹D. J. Morrissey, W. Benenson, E. Kashy, C. Bloch, M. Lowe, R. A. Blue, R. M. Ronningen, B. Sherrill, H. Utsunomiya, and I. Kelson, *Phys. Rev. C* **32**, 877 (1985).
- ²⁰D. J. Morrissey, C. Bloch, W. Benenson, E. Kashy, R. A. Blue, R. M. Ronningen, and R. Aryaeinjad, *Phys. Rev. C* **34**, 761 (1986).
- ²¹H. M. Xu, D. J. Fields, W. G. Lynch, M. B. Tsang, C. K. Gelbke, M. R. Maier, D. J. Morrissey, J. Pochodzalla, D. G. Sarantites, L. G. Sobotka, M. L. Halbert, D. C. Hensley, D. Hahn, and H. Stöcker, *Phys. Lett. B* **182**, 155 (1986).
- ²²C. B. Chitwood, C. K. Gelbke, J. Pochodzalla, Z. Chen, D. J. Fields, W. G. Lynch, R. Morse, M. B. Tsang, D. H. Boal, and J. C. Shillcock, *Phys. Lett. B* **172**, 27 (1986).
- ²³Z. Chen, C. K. Gelbke, J. Pochodzalla, C. B. Chitwood, D. J. Fields, W. G. Gong, W. G. Lynch, and M. B. Tsang, *Nucl. Phys.* **A473**, 564 (1987).
- ²⁴J. Pochodzalla, C. K. Gelbke, W. G. Lynch, M. Maier, D. Ardouin, H. Delagrange, H. Doubre, C. Gregoire, A. Kyanowski, W. Mittig, A. Peghaire, J. Peter, F. Saint-Laurent, B. Zwieglinski, G. Bizard, F. Lefebvres, B. Tamain, J. Quebert, Y. P. Viyogi, W. A. Friedman, and D. H. Boal, *Phys. Rev. C* **35**, 1695 (1987); J. Pochodzalla, W. A. Friedman, C. K. Gelbke, W. G. Lynch, M. Maier, D. Ardouin, H. Delagrange, H. Doubre, C. Gregoire, A. Kyanowski, W. Mittig, A. Peghaire, J. Peter, F. Saint-Laurent, Y. P. Viyogi, B. Zwieglinski, G. Bizard, F. Lefebvres, B. Tamain, and J. Quebert, *Phys. Lett.* **161B**, 275 (1985).
- ²⁵C. Bloch, W. Benenson, A. I. Galonsky, E. Kashy, J. Heltsley, L. Heilbronn, M. Lowe, B. Remington, D. J. Morrissey, and J. Kasagi, *Phys. Rev. C* **36**, 203 (1987).
- ²⁶D. Fox, D. A. Cebra, J. Karn, C. Parks, G. D. Westfall, and W. K. Wilson, *Phys. Rev. C* **36**, 640 (1987).
- ²⁷D. Fox, D. A. Cebra, Z. M. Koenig, P. Ugorowski, and G. D. Westfall, *Phys. Rev. C* **33**, 1540 (1986).
- ²⁸W. Bauer, *Nucl. Phys.* **A471**, 604 (1987).
- ²⁹D. H. Boal and J. C. Shillcock, *Phys. Rev. C* **33**, 549 (1986).
- ³⁰M. A. Bernstein, W. A. Friedman, W. G. Lynch, C. B. Chitwood, D. J. Fields, C. K. Gelbke, M. B. Tsang, T. C. Awes, R. L. Ferguson, F. E. Obenshain, F. Plasil, R. L. Robinson, and G. R. Young, *Phys. Rev. Lett.* **54**, 402 (1985).
- ³¹S. E. Koonin, *Phys. Lett.* **70B**, 43 (1977).
- ³²F. C. Barker and P. B. Treacy, *Nucl. Phys.* **38**, 33 (1962).
- ³³E. H. Berkowitz, G. L. Marolt, A. A. Rollefson, and C. P. Browne, *Phys. Rev. C* **4**, 1564 (1971).
- ³⁴F. D. Becchetti, C. A. Fields, R. S. Raymond, H. C. Bhang, and C. Overway, *Phys. Rev. C* **24**, 2401 (1981).
- ³⁵R. Hanbury-Brown and R. Q. Twist, *Nature* **178**, 1046 (1956).
- ³⁶C. Ezell, L. J. Gutay, A. T. Laasanen, F. T. Dao, P. Schübelin, and F. Turkot, *Phys. Rev. Lett.* **38**, 873 (1977).
- ³⁷D. Beavis, S. Y. Fung, W. Gorn, A. Huie, D. Keane, J. J. Lu, R. T. Poe, B. C. Shen, and G. VanDalen, *Phys. Rev. C* **27**, 910 (1983).
- ³⁸W. A. Zajc, J. A. Bisterlich, R. R. Bossingham, H. R. Bowman, C. W. Clawson, K. M. Crowe, K. A. Frankel, J. G. Ingersoll, J. M. Kurck, C. J. Martoff, D. L. Murphy, J. O. Rasmussen, J. P. Sullivan, E. Yoo, O. Hashimoto, M. Koike, W. J. McDonald, J. P. Miller, and P. Truöl, *Phys. Rev. C* **29**, 2173 (1984).
- ³⁹F. Zarbakhsh, A. L. Sagle, F. Brochard, T. A. Mulera, V. Perez-Mendez, R. Talaga, I. Tanihata, J. B. Carroll, K. S. Ganezer, G. Igo, J. Oostens, D. Woodard, and R. Sutter, *Phys. Rev. Lett.* **46**, 1268 (1981).
- ⁴⁰W. G. Lynch, C. B. Chitwood, M. B. Tsang, D. J. Fields, D. R. Klesch, C. K. Gelbke, G. R. Young, T. C. Awes, R. L. Ferguson, F. E. Obenshain, F. Plasil, R. L. Robinson, and A. D. Panagiotou, *Phys. Rev. Lett.* **51**, 1850 (1983).
- ⁴¹H. A. Gustafsson, H. H. Gutbrod, B. Kolb, H. Löhner, B. Ludewigt, A. M. Poskanzer, T. Renner, H. Riedesel, H. G. Ritter, A. Warwick, F. Weik, and H. Wieman, *Phys. Rev. Lett.* **53**, 544 (1984).
- ⁴²J. Bartke, M. Kowalski, V. G. Grishin, K. Miller, J. Pluta, T. Pawlak, W. Peryt, and Z. Strugalski, *Z. Phys. A* **324**, 471 (1986).
- ⁴³J. Pochodzalla, C. B. Chitwood, D. J. Fields, C. K. Gelbke, W. G. Lynch, M. B. Tsang, D. H. Boal, and J. C. Shillcock, *Phys. Lett. B* **174**, 36 (1986).
- ⁴⁴S. Nagamiya, *Phys. Rev. Lett.* **49**, 1383 (1982).
- ⁴⁵M.-C. Lemaire, S. Nagamiya, S. Schnetzer, H. Steiner, and I. Tanihata, *Phys. Lett.* **85B**, 38 (1982).
- ⁴⁶H. Sato and K. Yazaki, *Phys. Lett.* **98B**, 153 (1981).
- ⁴⁷C. Bloch, W. Benenson, E. Kashy, D. J. Morrissey, R. A. Blue, R. M. Ronningen, and H. Utsunomiya, *Phys. Rev. C* **34**, 850 (1986).
- ⁴⁸D. Hahn and H. Stöcker, *Phys. Rev. C* **35**, 1311 (1987).
- ⁴⁹D. Hahn and H. Stöcker, Lawrence Berkeley Laboratory Report No. LBL-21386, 1986.
- ⁵⁰C. Bloch, Ph.D. thesis, Michigan State University, 1987.